

EFFECT OF PRIMORDIAL BLACK HOLES ON THE COSMIC MICROWAVE BACKGROUND AND COSMOLOGICAL PARAMETER ESTIMATES

MASSIMO RICOTTI

Department of Astronomy, U of Maryland, College Park, MD 20742

JEREMIAH P. OSTRIKER AND KATHERINE J. MACK

Department of Astronomy, Princeton University;

Draft version February 1, 2008

ABSTRACT

We investigate the effect of non-evaporating primordial black holes (PBHs) on the ionization and thermal history of the universe. X-rays emitted by gas accretion onto PBHs modify the cosmic recombination history, producing measurable effects on the spectrum and anisotropies of the Cosmic Microwave Background (CMB). Using the third-year WMAP data and FIRAS data we improve existing upper limits on the abundance of PBHs with masses $> 0.1 M_{\odot}$ by several orders of magnitude.

Fitting WMAP3 data with cosmological models that do not allow for non-standard recombination histories, as produced by PBHs or other early energy sources, may lead to an underestimate of the best-fit values of the amplitude of linear density fluctuations (σ_8) and the scalar spectral index (n_s). Cosmological parameter estimates are affected because models with PBHs allow for larger values of the Thomson scattering optical depth, whose correlation with other parameters may not be correctly taken into account when PBHs are ignored. Values of $\tau_e \sim 0.2$, $n_s \sim 1$ and $\sigma_8 \sim 0.9$ are allowed at 95% CF. This result that may relieve recent tension between WMAP3 data and clusters data on the value of σ_8 .

PBHs may increase the primordial molecular hydrogen abundance by up to two orders of magnitude, this promoting cooling and star formation. The suppression of galaxy formation due to X-ray heating is negligible for models consistent with the CMB data. Thus, the formation rate of the first galaxies and stars would be enhanced by a population of PBHs.

Subject headings: cosmology: theory — cosmology: observations — early universe — cosmic microwave background — cosmological parameters — black hole physics

1. INTRODUCTION

During the radiation era, before the formation of the first stars and galaxies, small perturbations of the energy-density of the universe on scales comparable to the particle horizon may become gravitationally unstable. The outcome of the collapse can be the direct formation of primordial black holes (PBHs) (Hawking 1971; Carr & Hawking 1974a; Musco et al. 2005; Harada & Carr 2005). If these PBHs form at a sufficiently high mass, they do not evaporate but instead begin to grow by accretion, producing x-rays.

A population of sufficiently massive and numerous PBHs may provide an important and observable source of energy injection into the cosmic gas before the formation of non-linear large scale structures and galaxies. Several previous papers have addressed this scenario (Carr 1981; Gnedin et al. 1995; Miller & Ostriker 2001). Here, we improve on previous calculations by modelling the accumulation of dark matter around PBHs, the proper motion of PBHs and feedback effects including Compton drag. We simulate the ionization and thermal history of primordial plasma using semi-analytical calculations as in Ricotti & Ostriker (2004). The early energy injection by PBHs may produce observable distortions of the CMB spectrum (Battistelli et al. 2000) and may affect CMB anisotropies. We fit cosmological models which include the effect of PBHs on the cosmic recombination history

to the 3rd year WMAP data (Spergel et al. 2006). This is done by modifying the Monte-Carlo code COSMOMC (Lewis & Bridle 2002) appropriately. Our main goal is to improve existing upper limits on the mass and abundance of non-evaporating PBHs. In addition, we find that the existence of PBHs may affect the best fit estimates of cosmological parameters. In particular, the value of τ_e , σ_8 and n_s can be underestimated in models which do not account for the existence of PBHs. This result is more general than the case of PBHs discussed in this paper. Any source of energy injection at early time that modifies the recombination history may lead to underestimating τ_e , n_s and σ_8 if the effect is excluded a priori when fitting the WMAP3 data. This scenario may ease recent tensions between the WMAP3 analysis that favors low values of $\sigma_8 \sim 0.74$ (assuming a standard recombination history) and clusters data that may favor larger values of $\sigma_8 \sim 0.9$ (Evrard et al. 2007), but see also (Bode et al. 2007).

Finally, ionization from the X-rays of accreting PBHs will increase the amount of H_2 significantly and the resultant extra cooling will enhance early star formation.

This paper is organized as follows. In § 2 we review the properties of PBHs and the current constraints. In § 3 we introduce the basic equations for gas and dark matter accretion and for the accretion luminosity of PBHs. In § 4 we evaluate the effect of local and global feedback processes. In § 5 we present the results of calculations of the ionization and thermal history of the IGM and

in § 6, data from WMAP3 and COBE are used to constrain the mass and abundance of PBHs. A summary and discussion is presented in § 7. Throughout the rest of the paper we use the following cosmological parameters ($h = 0.73, \Omega_m = 0.238, \Omega_b = 0.0418, \sigma_8 = 0.74, n_s = 0.95$) from WMAP3 (Spergel et al. 2006).

2. PRIMORDIAL BLACK HOLES

In the Newtonian regime, the theory of PBH formation can be understood in simple terms. The Jeans length in a static and homogeneous fluid with sound speed v_s is $R_J \sim (c/v_s)R_{Sch}$, where R_{Sch} is the Schwarzschild radius of a black hole with density equal to the mean cosmic value. During the radiation era $v_s \approx c/\sqrt{3}$, thus $R_J \rightarrow R_{Sch}$. This means that the self-gravitating regime appears when the perturbation is very close to the black hole regime. The critical overdensity needed to trigger PBH collapse is $w \lesssim 1/3$, where $P = w\rho c^2$ is the cosmic equation of state (Carr 1975; Green et al. 2004). The typical mass of a PBH is approximately equal to or smaller than the mass within the particle horizon at the redshift of its formation, z_f :

$$\frac{M_{pbh}}{M_H(z_{eq})} \sim f_{Hor} \left(\frac{1+z_{eq}}{1+z_f} \right)^2 \sim f_{Hor} \left(\frac{\beta}{\Omega_{pbh}} \right)^2. \quad (1)$$

Here, $f_{Hor} = M_{pbh}/M_H(z_f) \leq 1$ is the ratio of the mass of the PBH to the mass of the particle horizon at $z = z_f$, β is the density parameter of PBHs at $z = z_f$, $M_H(z_{eq}) \sim 3.1 \times 10^{16} M_\odot$ is the mass of the horizon at the redshift of matter-radiation equality $z_{eq} \approx 3000$ (for $\Omega_m h^2 = 0.127$, Spergel et al. 2006). The relationship $\beta(1+z_f) = \Omega_{pbh}(1+z_{eq})$, valid for non-evaporating PBHs, relates the density parameter of PBHs today, $\Omega_{pbh}(M) = \rho_{pbh}/\rho_{crit}$, to the one at the time of formation, $\beta(M)$. For example, if a tiny fraction $\beta \sim 10^{-9}$ of the cosmic energy-density collapses into PBHs during the quark-hadron phase transition at $t \sim 10^{-5}$ s, it follows from equation (1) that about 30% of the present day dark matter is made of PBHs with mass $M_{pbh} \sim 1 M_\odot$ (we assumed $f_{Hor} = 1$). Nothing prevents the dark matter from being a mixture of weakly interacting particles (WIMPs) and PBHs with $\Omega_{dm} = \Omega_{pbh} + \Omega_{wimp}$. However, equation (1) shows that fine tuning of the value of β is required in order to have $\Omega_{pbh} \sim \Omega_{wimp}$. Thus, it is often considered more likely that dark matter is dominated by either WIMPs or PBHs. PBHs may have an extended mass range if they form at different epochs and, even if they all form at one epoch, simulations show that their mass distribution is broad (e.g., Choptuik 1993; Evans & Coleman 1994). Thus, present-day dark matter may be composed of a mixture of relatively massive and tiny PBHs, some of which may be completely evaporated or have left Planck-mass relics. In practice, using astrophysical tests only, sufficiently small PBHs would be virtually indistinguishable from WIMPs. It is worth pointing out that no fine tuning of $\beta(z_f)$ is required to produce $\Omega_{dm} = \Omega_{pbh} \sim 1$. Any value of $\beta \leq 1$ and z_f is allowed but, of course, different values of the entropy of the Universe and different redshift of equivalence would be produced. Specifically, the radiation density parameter today is related to β and z_f by the relationship $\Omega_{rad,0} = \Omega_{dm}/(1+z_{eq}) \sim \beta^{-1}(1+z_f)^{-1}$. In addition, a scenario in which PBHs produced after inflation evaporate leaving only Planck mass relics may

explain why $\Omega_{rad,0} h^2 \sim 4.35 \times 10^{-5}$ and provide a justification for the large value of the entropy of the Universe (Alexander & Mészáros 2007).

PBHs are a unique probe of the early universe, of high energy processes and of quantum gravity. The small mass scales at which PBHs may form are inaccessible to Cosmic Microwave Background (CMB) experiments. As of today there is no solid evidence for the existence of PBHs, but their presence would be very difficult to detect even if they constitute the bulk of the dark matter. Early results from the MACHO collaboration (Alcock et al. 2000) suggested a possible detection of solar mass objects constituting about 20% of the Galactic halo mass. Recent results seem to disfavor this claim (e.g., Hamadache et al. 2006). The goal of the present work is to better constrain the abundance of relatively massive ($M \gtrsim 0.1 M_\odot$) PBHs by modeling their effect on the ionization history of the universe. To further motivate the present study we briefly review the current status of theoretical works and observational limits on the existence of PBHs. For a more comprehensive review see Carr (2005).

2.1. Current observational limits on PBHs

Many physical processes may lead to the formation of PBHs. For example, PBHs may form from perturbations after inflation, during phase-transitions of the cosmic equation of state or from topological defects (Carr & Hawking 1974b; Carr 2005, e.g.). Theoretically, it is unclear what is the largest allowed mass of PBHs. Inflationary theories predict an almost scale-invariant ($n \sim 1$) initial spectrum of perturbations. This spectrum has the remarkable property that all perturbations have the same amplitude when they enter the horizon. Thus, in this case, it may appear that the probability of PBH formation is almost independent of their mass. Small-mass PBHs would have a larger probability of formation if the spectrum were slightly blue (with $n > 1$) and vice versa if the spectrum were red, as seems to be indicated by available data (Spergel et al. 2006; Chongchitnan & Efstathiou 2007). Jedamzik (1997) have shown that during a first-order phase transition the cosmic equation of state may become softer ($w \ll 1/3$). As a result, the formation of PBHs may be substantially enhanced at that particular mass scale. PBHs with masses $\sim 1 M_\odot$ may form during the QCD (quark-hadron) phase transition at $t \sim 10^{-5}$ s, or PBHs with mass $10^5 M_\odot$ may form during $e^+ - e^-$ annihilation era. PBHs with masses of $100 - 1000 M_\odot$ may be produced in two-stage inflationary models designed to fit the low WMAP quadrupole (Kawasaki et al. 2006). One interesting feature of this model is a huge bump in the power spectrum at kpc scales with overdensity $\delta > 1$. Other possible scenarios for PBH formation involve non-Gaussian perturbations produced by cosmic strings, cosmic string collapse or bubble collisions following second-order phase transitions (e.g., Polnarev & Zembowicz 1991; Rubin et al. 2001; Stojkovic et al. 2005; Nozari 2007). It is generally considered unlikely that PBH formation occurred after $t = 1$ s, when $M_{pbh} \sim M_H \gtrsim 10^5 M_\odot$, because the physics in this domain is sufficiently understood and their formation would affect primordial nucleosynthesis.

Observationally, the abundance of PBHs is well constrained only at very small masses. PBHs with masses

smaller than 5×10^{14} g should not exist today because they evaporate in less than a Hubble time by emission of Hawking radiation (Hawking 1974). The radiation from evaporating PBHs affects nucleosynthesis and the CMB spectrum and may overproduce the observed gamma-ray background. Hence, upper limits on the abundance of PBHs with masses $1 \text{ g} < M_{pbh} < 10^{15} \text{ g}$ are quite stringent: $\beta(M) \sim 10^{-20} - 10^{-22}$ (e.g. Carr 2003). The number density of PBHs with masses larger than 10^{15} g is poorly constrained because they emit negligible amounts of Hawking radiation (their timescale for evaporation is longer than the age of the Universe today). Dynamical constraints (Lacey & Ostriker 1985; Carr 1994; Moore 1993; Jin et al. 2005), effects on the matter power spectrum (Afshordi et al. 2003) and statistical studies of binary stars in the Galactic halo (Yoo et al. 2004), have been used to rule out PBHs more massive than $1000 M_{\odot}$ as main constituent of the dark matter, but (Mack et al. 2007, hereafter Paper I), summarizing these constraints, find that a domain remains for which massive PBHs can make a significant contribution to the dark matter. Searches for microlensing events toward the Large Magellanic Cloud by the MACHO and EROS collaborations so far provide the most stringent constraints on the existence of non-evaporating PBHs. They have ruled out PBHs as the bulk of the galactic dark matter in the mass range $10^{-7} M_{\odot} < M < 30 M_{\odot}$ (Alcock et al. 1998, 2001). Alcock et al. (2000) have claimed a positive detection of Massive Compact Halo Objects (MACHOs) with $M \sim 0.1 - 1 M_{\odot}$ constituting about 20% of the Milky-Way dark matter halo. More recent works have not confirmed this result (Hamadache et al. 2006) but this mass range is of particular interest because it is about the mass of PBHs that may form during quark-hadron phase transition as proposed by (Jedamzik 1997). The gray curves in Figure 9(left) summarize the current status of observational upper limits on the abundance of PBHs with $M_{pbh} > 10^{15} \text{ g}$. The two black curves labeled “FIRAS” and “WMAP3” show the new upper limits derived in the present work.

2.2. PBH growth and “clothing” dark halo

PBHs more massive than $10^5 M_{\odot}$ may only exist if substantial accretion takes place after their formation or if many PBHs which form in a cluster merge into a larger one (Meszaros 1975a; Khlopov et al. 2005; Chisholm 2006). In the Newtonian approximation, PBHs can only grow if their mass is comparable to the horizon mass. In this case their mass increases at the same rate as the horizon mass (Zel’Dovich & Novikov 1967). Relativistic calculations by Carr & Hawking (1974b) have shown that growth by accretion is always slower than the growth of the horizon mass. Thus, it is generally accepted that the mass of PBHs does not increase significantly after their formation. In models in which the equation of state becomes stiff $w \sim 1$ (Lin et al. 1976) or in brane world cosmologies in which extra dimensions are sufficiently large, growth by accretion could be significant and in principle may lead to the production of massive PBHs starting from smaller seeds (Bicknell & Henriksen 1978; Guedens et al. 2002a,b; Majumdar 2003; Tikhomirov & Tsalkou 2005).

Scenarios in which the bulk of the dark matter is not made of PBHs are particularly interesting because, after

the redshift of matter-radiation equivalence, each PBH seeds the growth of a dark halo that, over time, becomes considerably more massive than the PBH in its center (Paper I). The halo gravitational potential may increase the gas accretion rate onto the central PBH by several orders of magnitude. If the accretion is near the Eddington rate, the radiation efficiency of PBHs may be large. At later times, when PBHs are accreted by the massive halos of galaxies, they likely lose much of their dark matter “clothing” and become “naked” again.

3. BASIC EQUATIONS

Here we review the theoretical framework for the accretion of dark matter and baryons by primordial black holes. A point mass, M , immersed in an hydrogen gas with constant number density n_{gas} and sound speed c_s that moves at velocity v with respect to the gas accretes at a rate

$$\dot{M}_b = \lambda 4\pi m_H n_{gas} v_{eff} r_B^2,$$

where $r_B \equiv GMv_{eff}^{-2}$ is the Bondi-Hoyle radius and $v_{eff} \equiv (v^2 + c_s^2)^{1/2}$ (Bondi & Hoyle 1944). The numerical values of the Bondi radius and accretion rate are:

$$r_B \approx 1.3 \times 10^{-4} \text{ pc} \left(\frac{M}{1 M_{\odot}} \right) \left(\frac{v_{eff}}{5.7 \text{ km s}^{-1}} \right)^{-2}, \quad (2)$$

$$\dot{M}_b \approx 2 \times 10^{12} \text{ g s}^{-1} \lambda n_{gas} \left(\frac{M}{1 M_{\odot}} \right)^2 \left(\frac{v_{eff}}{5.7 \text{ km s}^{-1}} \right)^{-3} \quad (3)$$

The mean cosmic gas density is

$$n_{gas} \simeq 200 \text{ cm}^{-3} \left(\frac{1+z}{1000} \right)^3. \quad (4)$$

Before decoupling the gas temperature is roughly equal to the temperature of the CMB. Afterwards the gas temperature decreases adiabatically due to the Hubble expansion of the Universe. The temperature of the IGM (neglecting for the moment the feedback produced by accreting PBHs) is well approximated by the fitting formula

$$T_{gas} = (2730 \text{ K}) \left(\frac{z+1}{1000} \right) \frac{a_{dec}}{(a^{\beta} + a_{dec}^{\beta})^{1/\beta}}, \quad (5)$$

where $a \equiv 1/(1+z)$ is the scale parameter, a_{dec} is the scale parameter at decoupling where $z_{dec} \simeq 132(\Omega_b h^2/0.022)^{2/5}$ and $\beta = 1.72$. The gas sound speed is $c_s = (5.7 \text{ km s}^{-1})(T_{gas}/2730)^{1/2}$. Thus, from equation (5) we have

$$c_s \approx (5.7 \text{ km s}^{-1}) \left(\frac{1+z}{1000} \right)^{1/2} \text{ for } z \gg z_{dec} \sim 132. \quad (6)$$

For spherical accretion onto a point mass, assuming a non-viscous fluid, the parameter λ is of order unity. In the present study, we need to take into account the effects of the growth of a dark halo around PBHs, the Hubble expansion and the coupling of the CMB radiation to the gas through Compton scattering (Compton drag). All these effects can be folded into the calculation of the accretion eigenvalue λ . In a companion paper, (Ricotti 2007, hereafter Paper II), we have derived analytical relationships for λ for the cases of a point mass and an extended dark halo, including the aforementioned cosmological effects.

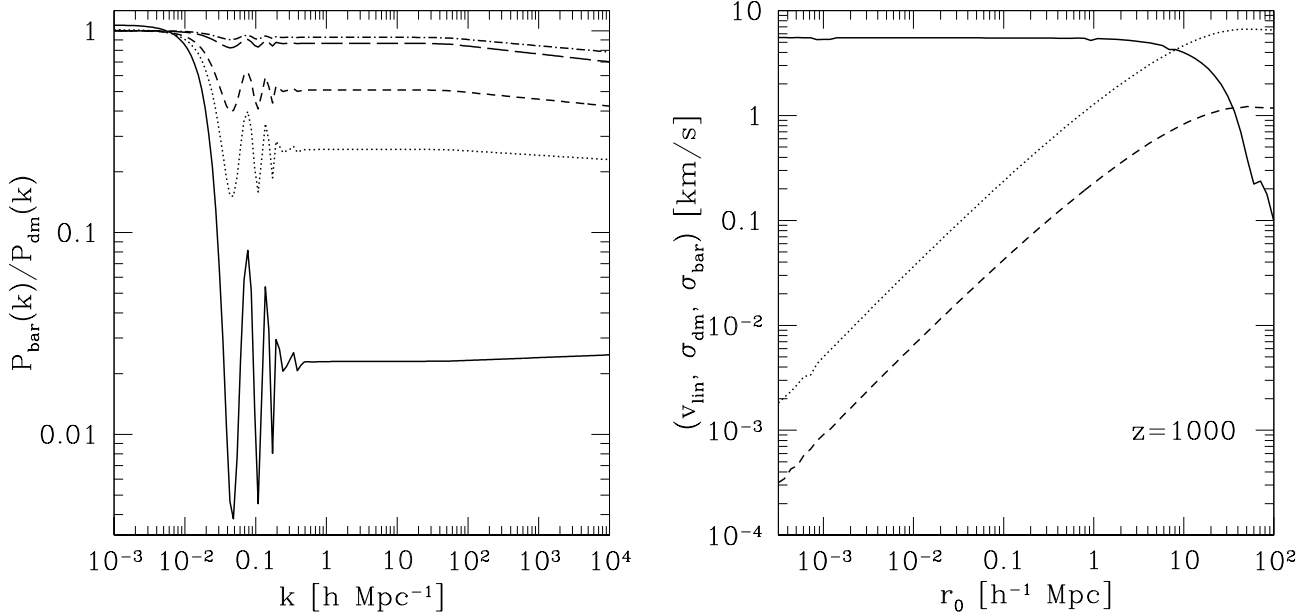


FIG. 1.— (Left). Ratio of the baryonic to dark matter power spectrum as a function of wavenumber k . Each curve, from bottom to the top, corresponds to scale factors $a = 0.001, 0.002, 0.005, 0.01, 0.05, 0.1$, respectively. (Right). The solid curve shows the mean relative velocity between the dark matter and baryons in a sphere of comoving radius r_0 . The dashed and dotted curves show the velocity dispersion within a sphere of comoving radius r_0 for the baryons and for the dark matter, respectively.

In the following calculations we will use the results from Paper II to derive the accretion rate onto “naked” PBHs (appropriate only if PBHs constitute the bulk of the dark matter) and for the general case of accretion onto PBHs including the growth of a “clothing” dark halo of mass M_h .

To obtain this result, we must first estimate the dark matter accretion (§3.1) and the effects of PBH velocity (§3.2), the angular momentum (§3.3) of the dark and baryonic matter and PBH clustering (§3.4). From the gas accretion rate, we can then estimate the accretion luminosity, which will ultimately be responsible for altering the evolution of the IGM.

3.1. Growth of a dark halo around PBHs

If PBHs do not constitute the bulk of the dark matter, they seed the accumulation of a dark halo of WIMPs which grows proportionally to $t^{2/3}$ (Bertschinger 1985; Mack et al. 2007). A similar result holds if the dark matter is made only of PBHs but with a very broad distribution of masses.

After the redshift of equivalence the mass of the dark halo surrounding PBHs grow proportionally to the cosmic scale parameter:

$$M_h(z) = \phi_i M_{pbh} \left(\frac{z+1}{1000} \right)^{-1}, \quad (7)$$

where $\phi_i = 3$ (see Paper I). The growth of the PBH during the radiation era is of order of unity. After $z \sim 30$, depending on the environment, the dark halo may stop growing: if a PBH evolves in isolation it can continue to grow, otherwise it will lose mass due to tidal forces as it is incorporated into a larger galactic dark halo.

If $M_h > M_{pbh}$ and the accretion is not perfectly spherical, the dark halo has a self-similar power-law density profile $\rho \propto r^\alpha$ with $\alpha \sim -2.25$ (Bertschinger 1985) trun-

cated at a halo radius

$$r_h = 0.019 \text{ pc} \left(\frac{M_h}{1 M_\odot} \right)^{1/3} \left(\frac{1+z}{1000} \right)^{-1}, \quad (8)$$

where r_h is about one third of the turn-around radius (Paper I and II).

3.2. Proper motions of PBHs

The motion of the accreting mass relative to the surrounding material strongly affects the accretion rate (see equation [3]). This proper motion is determined by the relative amplitude of inhomogeneities of dark matter and gas. More precisely, assuming that PBHs behave like dark matter particles and neglecting binary interactions, we estimate their relative velocity with respect to the gas in the linear and non-linear regimes. We show that at redshifts $z \gtrsim 30 - 50$, due to the imperfect coupling of gas and dark matter perturbations (*i.e.*, Silk damping), the peculiar velocity of PBHs with respect of the gas is of the order of the gas sound speed. At redshifts $z < 30$ the growth of non-linear perturbations dominates the motion of PBHs. The velocity of PBHs falling into the potential wells of the first galaxies is sufficiently large to virtually stop the accretion of gas from the intergalactic medium onto PBHs, until they came to rest at the center of the halo into which they are accreted.

3.2.1. Linear regime

In linear theory, gas and dark matter perturbations are coupled. Before the redshift of “decoupling” at $z \sim 100$, the growth of gas inhomogeneities on small scales is suppressed by Silk damping (Silk 1968). At these scales and redshifts, the gas flow lags behind the dark matter until it is able to catch up at later times. This process is illustrated quantitatively in the left panel of Fig. 1, which shows the ratio of the gas to dark matter power spectra in our fiducial Λ CDM model. The curves, from

bottom to the top, show the ratio of the power spectra of the baryons to dark matter calculated using the code “lingers” in the Graphic1 package (Bertschinger 1985) at scale parameters $a = 0.001, 0.005, 0.01, 0.05,$ and $0.1,$ respectively.

From the power spectra of dark matter and baryons we calculate the ensemble average of the center-of-mass velocity of a patch of the universe of comoving radius r_0 (Ostriker & Suto 1990):

$$\langle V_i \rangle^2 = \frac{\Omega_m^{1.2} H^2}{2\pi^2} \int_0^\infty P_i(k) w_s^2(k, a) w_l^2(k, r_0) dk, \quad (9)$$

where Ω_m is the cosmological density parameter, w_s and w_l are window functions (here we use “top hat” window functions) and a is a small scale smoothing of the perturbations. The choice of the value of a is not critical as long as $a \ll r_0$. The index $i = dm, bm$ refers to dark matter and baryons, respectively. The ensemble average of the velocity variance within a patch of comoving radius r_0 is calculated in a similar fashion:

$$\langle \sigma_i \rangle^2 = \frac{\Omega_m^{1.2} H^2}{2\pi^2} \int_0^\infty P_i(k) w_s^2(k, a) [1 - w_l^2(k, r_0)] dk. \quad (10)$$

This equation will be used later (§ 3.3) to estimate the angular momentum of gas and dark matter accreting onto PBHs. The “cosmic Mach number,” $\mathcal{M}_i = \langle V_i \rangle / \langle \sigma_i \rangle$, is independent of the uncertainties on the normalization of the power spectrum (Ostriker & Suto 1990).

Since the flow of the gas and the dark matter trace each other, their mean relative velocity is $\langle V_{rel} \rangle \equiv \langle V_{dm} \rangle - \langle V_{bar} \rangle$. The right panel of Fig. 1 shows the mean relative velocity $\langle V_{rel} \rangle$ of PBHs with respect to the baryons (solid curves), and the velocity dispersion $\langle \sigma_{dm, bm} \rangle$ for the gas (dashed curve) and the dark matter (dotted curve) within a sphere of comoving radius r_0 at $z = 1000$. Power-law fits for $\langle \sigma \rangle$ as a function of r_0 and z are:

$$\sigma_{bm} \approx (0.35 \text{ km s}^{-1}) \left(\frac{r_0}{1 \text{ Mpc}} \right)^{0.85} \left(\frac{1+z}{1000} \right)^{-1}, \quad (11)$$

$$\sigma_{dm} \approx (1.58 \text{ km s}^{-1}) \left(\frac{r_0}{1 \text{ Mpc}} \right)^{0.85} \left(\frac{1+z}{1000} \right)^{-\frac{1}{2}}. \quad (12)$$

The fits are accurate to about 5% for $r_0 < 1$ Mpc in the redshift range $50 < z < 2000$.

In § 3.6 we discuss in more detail the radiative efficiency of accreting PBHs. We anticipate that the radiative efficiency ϵ and the accretion luminosity L depend on the accretion rate \dot{m} : $L \propto v_{eff}^{-6}$ if $\dot{m} < 1$ and $L \propto v_{eff}^{-3}$ if $\dot{m} \gtrsim 1$, where the effective velocity v_{eff} is defined in § 3 (see equation [3]). The effect of the linear velocity field, which is Gaussian, on the mean accretion luminosity of PBH is given by the statistical ensemble average of $v_{eff}^{-\alpha}$ weighted by the distribution function of the PBHs relative velocities with respect to the gas:

$$\langle v_{eff}^{-\alpha} \rangle = \int_0^\infty \frac{f_M(v, \sigma) dv}{(c_s^2 + v^2)^{\alpha/2}}, \quad (13)$$

where $\alpha = 3$ or $\alpha = 6$, depending on the value of the accretion rate. The linear velocity field is Gaussian; thus the distribution of the moduli of the 3D velocity field is

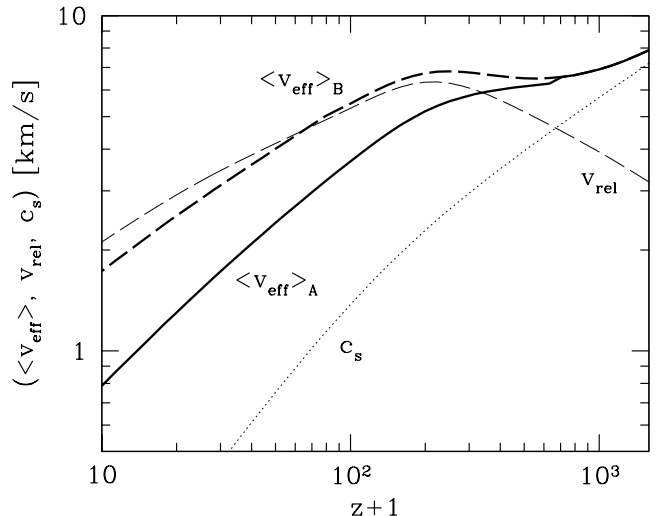


FIG. 2.— Luminosity weighted effective velocity of PBHs (thick curves): $\langle v_{eff} \rangle_A$ (solid curve), is weighted assuming $l \propto \dot{m}^2$ and $\langle v_{eff} \rangle_B$ (dashed curve), is weighted assuming $l \propto \dot{m}$. See the text for details. The thin curves show the variance of the velocity distribution, $\langle V_{rel} \rangle$ (dashed line) and the gas sound speed, c_s (dotted line), respectively.

a Maxwellian, $f_M(v, \sigma)$ with $\sigma = \langle V_{rel} \rangle$. Finally, integrating equation (13) and defining $\mathcal{M}_{pbh} = \langle V_{rel} \rangle / c_s$, we find

$$\langle v_{eff} \rangle_A \approx \begin{cases} \langle c_s \rangle \left[\frac{16}{\sqrt{2\pi}} \mathcal{M}_{pbh}^3 \right]^{\frac{1}{6}} & \text{for } \mathcal{M}_{pbh} > 1, \\ c_s (1 + \mathcal{M}_{pbh}^2)^{\frac{1}{2}} & \text{for } \mathcal{M}_{pbh} < 1, \end{cases} \quad (14)$$

for $\alpha = 6$ and

$$\langle v_{eff} \rangle_B \approx \begin{cases} c_s \mathcal{M}_{pbh} \left[\sqrt{\frac{2}{\pi}} \ln \left(\frac{2}{e} \mathcal{M}_{pbh} \right) \right]^{-\frac{1}{3}} & \text{for } \mathcal{M}_{pbh} > 1, \\ c_s (1 + \mathcal{M}_{pbh}^2)^{1/2} & \text{for } \mathcal{M}_{pbh} < 1, \end{cases} \quad (15)$$

for $\alpha = 3$. The calculations presented in this section on the effect of linear perturbations on the accretion luminosity of PBHs are summarized in Fig. 2. The thick solid and dashed curves show $\langle v_{eff} \rangle_B$ from equation (15), and $\langle v_{eff} \rangle_A$ from equation (14) respectively, as a function of redshift. For comparison, the thin dashed and dotted curves show $\langle V_{rel} \rangle$ and the sound speed of the gas, respectively. Neglecting feedback effects, the PBH velocity is comparable to the gas sound speed at redshifts $z \lesssim 500$. On average, the motion of PBHs in the linear regime reduces the gas accretion rate by a factor of a few with respect to the static case.

3.2.2. Non-linear regime

The velocity of PBHs falling into the gravitational potential of nearby galactic halos can be roughly estimated assuming that it is comparable to the circular velocity of virialized halos of 2σ density perturbations: $v_p \sim v_c(2\sigma, z)$. We calculate $v_c(2\sigma, z)$ using the Press-Schechter formalism (Press & Schechter 1974). Adopting a top-hat window function to calculate the variance of density perturbations, we find $\sigma(M) \approx 10.2 - 0.79 \log(M)$ for masses $M < 10^{10} M_\odot$. Hence, for the mass range of interest,

$$M_{2\sigma} = (8.8 \times 10^{12} M_\odot) \exp[-1.8(z+1)], \quad (16)$$

is a sufficiently accurate approximation for the mass of 2σ perturbations as a function of redshift. From equation (16) we calculate the circular velocity and thus typical proper velocity of PBHs induced by non-linear structures, as a function of redshift:

$$v_p \sim v_c = (17 \text{ km s}^{-1}) \left(\frac{M_{2\sigma}}{10^8 M_\odot} \right)^{\frac{1}{3}} \left(\frac{z+1}{10} \right)^{\frac{1}{2}}. \quad (17)$$

The fraction of the dark matter and hence of PBHs in virialized halos with mass $> M_{min}$ is $f_{vir}(z) = 1 - \text{erf}(\nu_{min}/\sqrt{2})$, where erf is the error function and $\nu = \delta_c/\sigma(M_{min}, z)$. For a fraction f_{vir} of PBHs we assume that they have a velocity v_p relative to the gas and that the gas has overdensity $\delta = 200$. The remaining PBHs are in the intergalactic medium and are subject to global and local thermal feedback (see § 4).

Dynamical friction may allow the most massive PBHs to spiral to the center of the halos in less than a Hubble time (see § 7), where they meet favorable conditions for accretion. For smaller PBHs inside virialized halos, their contribution to the accretion luminosity is important only in the redshift range $10 \lesssim z \lesssim 30$. At $z > 30$ the fraction of PBHs in virialized halos is small. At $z < 10$, the first massive halos form and the rate of gas accretion onto PBHs decreases rapidly due to the increasing relative velocity of the PBHs with respect to the gas: $v_c \gtrsim 10 \text{ km s}^{-1}$. During this redshift interval only a fraction $\sim 10 - 20\%$ of PBHs is inside virialized halos. Most PBHs at $z \sim 10$ are still in the intergalactic medium. The gas accretion onto the PBHs in the intergalactic medium is strongly suppressed at $z < 10$ due to global thermal feedback (see Fig. 6).

3.3. Angular momentum of accreted material

The angular momentum of the accreting gas determines whether a disk forms or the accretion is quasi-spherical. In turn, the geometry of gas accretion determines the radiative efficiency $\epsilon(\dot{m})$, *i.e.*, the efficiency of conversion of gravitational energy into radiation (see § 3.6). The angular momentum of accreting dark matter determines the density profile of the dark halo enveloping a PBH and whether the mass of a PBH can grow substantially by accreting a fraction of its enveloping dark halo. The angular momentum of the gas and dark matter accreting onto PBHs can be estimated from equation (12) for the mean values of the velocity dispersion within a comoving volume of radius r_0 (see right panel of Fig. 1). For the gas we estimate $\sigma_{bm}(r_{B,com})$ at the Bondi radius (see equation [3]), and for the dark matter we estimate $\sigma_{dm}(r_{h,com})$ at the turn-around radius (see equation [8]). If we neglect the proper motion of PBHs, the Bondi radius of a “naked” PBH is approximately constant at redshifts $z < 100$: $r_{B,com} \sim (1.3 \times 10^{-7} \text{ Mpc})(M_{pbh}/1M_\odot)$. The proper motion of PBHs produces a small reduction of the Bondi radius that we parameterize with the function $\xi(z) = \max[\mathcal{M}_{pbh}(z), 1]$, where $\mathcal{M}_{pbh} = \langle v_{eff} \rangle / c_s$, is the PBH Mach number. Replacing M_h with the mass of the PBH in the previous expression, we obtain an estimate of the Bondi radius including the enveloping dark halo. Finally, from equation (12) we obtain

$$\sigma_{bm} \approx \sigma_{bm,0} \xi(z)^{-1.7} \left(\frac{1+z}{1000} \right)^{-1} \left(\frac{M_h}{1 M_\odot} \right)^{0.85}, \quad (18)$$

$$\sigma_{dm} \approx \sigma_{dm,0} \left(\frac{1+z}{1000} \right)^{-\frac{1}{2}} \left(\frac{M_h}{1 M_\odot} \right)^{0.28}, \quad (19)$$

where $\sigma_{bm,0} = 3.8 \times 10^{-7} \text{ km s}^{-1}$ and $\sigma_{dm,0} = 1.4 \times 10^{-4} \text{ km s}^{-1}$.

Let’s first consider the accretion geometry of the gas. Applying conservation of angular momentum we find that the rotational (*i.e.*, tangential) velocity of the gas at a distance r from the black hole is $v(r)r \sim \sigma_{bm}r_B$, where r_B is the Bondi radius. Neglecting relativistic effects, if the velocity is much smaller than the Keplerian velocity in the proximity of the black hole, then the accretion is quasi-spherical; if vice versa, a disk can form. The Keplerian velocity at radius r is $v_{kep} = c(R_{Sch}/r)^{1/2} < c$, where $R_{Sch} = 2GM/c^2$ is the Schwarzschild radius of the PBH ($R_{Sch} \sim 3 \text{ km}$ for a $1 M_\odot$ black hole). Thus, the gas accretion is quasi-spherical if $\sigma_{bm} < 2D\xi(z)^2 c_s^2/c$. We have assumed $c_s \propto (1+z)^{1/2}$ and the constant $D \sim 1 - 10$ takes into account relativistic corrections. We conclude that the angular momentum of the gas is negligible when the halo mass is

$$M_h < (1746 M_\odot) D^{1.17} \xi(z)^{4.33} \left(\frac{1+z}{1000} \right)^{2.35}. \quad (20)$$

Using $\mathcal{M}_{pbh}(z)$ calculated in § 3.2.1 and $D = 10$, the flow is quasi-spherical for any halo mass $M_h \lesssim (1700 - 17000) M_\odot$, almost independently of redshift. At redshifts $z < 100$, the dark halo mass is about 30 times the mass of the PBH in its center. We conclude that an accretion disk forms at redshifts $z < 100$ around PBHs more massive than $M_{pbh} \sim 500 M_\odot$. Thermal feedback effects, which are important at $z < 100$, will increase our simple estimate of the critical mass for disk formation. So far we did not take into account feedback effects and Compton drag which are important in reducing the gas angular momentum. Previous studies have found that due to Compton drag the flow is nearly spherical at redshifts $z > 100$ (*e.g.*, Loeb 1993; Umemura et al. 1993).

Similar arguments apply to the dark matter component. The flow is sufficiently spherical for the dark matter to be directly accreted onto the PBH if $\sigma_{dm} < cDR_{Sch}/r_h$. This inequality is satisfied for PBHs with masses

$$M_{pbh} > (7.18 \times 10^5 M_\odot) D^{-2.6} \left(\frac{1+z}{1000} \right)^{-2.9}, \text{ or} \\ \frac{M_{pbh}}{M_H} > (7.76 \times 10^{-13}) D^{-2.6} \left(\frac{1+z}{1000} \right)^{-0.9}, \quad (21)$$

in terms of the Horizon mass $M_H(z)$. Including relativistic corrections ($D \sim 10$), only PBHs with mass $\gtrsim 10^3 M_\odot$ at $z \sim 1000$ (note the steep dependence of the critical mass on redshift) may grow substantially from direct accretion of dark matter. The geometry of the dark halo becomes more spherical with the increasing mass of the PBH, since the ratio of the halo radius to the Schwarzschild radius, $r_h/R_{sw} \propto M_{pbh}^{-2/3}$, decreases with increasing mass. We conclude that direct accretion of dark matter into PBHs is typically negligible. In most cases the density profile of the dark halo is well described by the Bertschinger self-similar solution with log slope $\alpha = 2.25$.

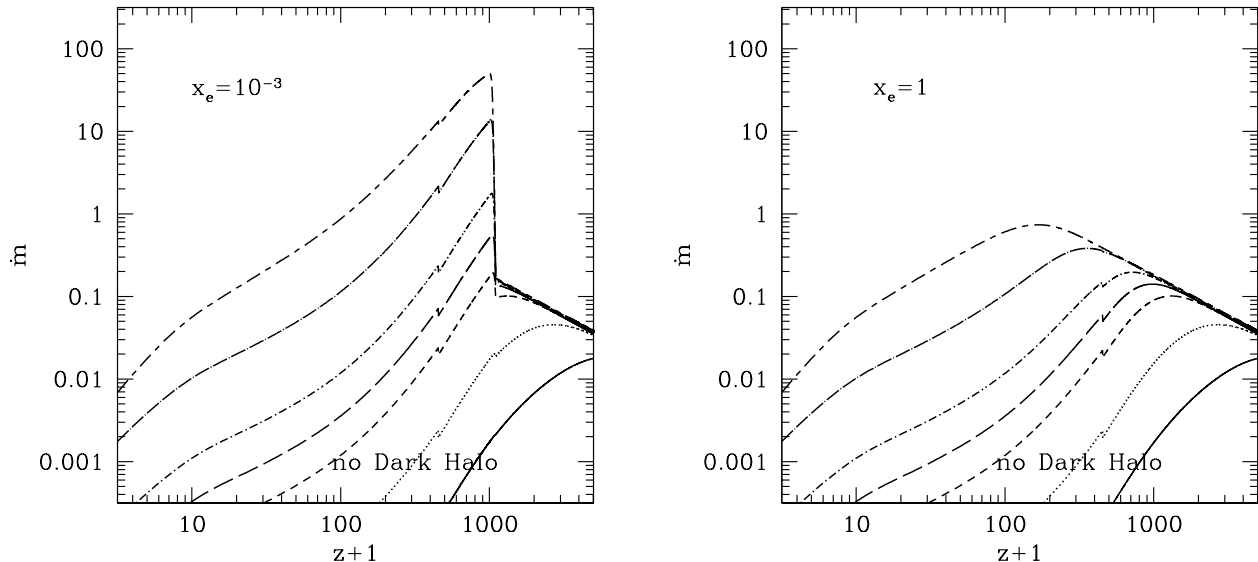


FIG. 3.— The dimensionless accretion rate of baryonic matter onto a “naked” PBH (without enveloping dark halo) as a function of redshift. The curves from bottom to top refers to $M_{pbh} = 1, 10, 100, 300, 10^3, 10^4, 10^5 M_\odot$. The *left* panel is for a gas with electron fraction $x_e = 10^{-3}$; the *right* panel for $x_e = 1$. Here, thermal feedback and the contribution from PBHs inside virialized halos are neglected. The motion of the PBH due to linear density perturbations is included.

3.4. PBHs Clustering

Recently it has been suggested by several authors (*e.g.*, Dokuchaev et al. 2004; Carr 2005; Chisholm 2006) that PBHs have high probability of forming clusters or binaries. A precise calculation of the effect of clustering is complex and beyond the scope of the present paper. Nevertheless, there are simple arguments that we can use to show that clustering may increase the radiative efficiency of PBHs.

We consider two regimes determined by the relationship between the typical size of the cluster (or the binary separation), r_{cl} , and the Bondi radius of the whole system, $r_{B,tot}$.

1) If $r_{cl} > r_{B,tot}$, the orbital velocities of the PBHs are smaller than the effective translational velocity of the system. Hence, we can neglect the orbital velocities to estimate the accretion rate. To a first approximation in this case, we can ignore the fact that the PBHs are clustered or in binary systems for the purpose of calculating their accretion luminosity.

2) If $r_{cl} < r_{B,tot}$, the orbital velocities of the PBHs are larger than the effective translational velocity of the system. Thus, the material is not accreted directly onto the PBHs but near the center of mass of the system and subsequently onto the PBHs. Because the PBHs are orbiting the center of mass of the cluster, the angular momentum of the accreted material is large and so the accretion geometry is disk-like rather than spherical. The formation of a disk can increase the radiative efficiency by a factor of ten (see §3.6). Further work is needed to better understand the accretion rate of PBHs in this regime.

3.5. Gas accretion rate

We now have all that is needed to estimate the accretion rate onto PBHs from equation (3). We define the dimensionless accretion luminosity $l \equiv L_{bol}/L_{Ed}$, where $L_{Ed} \equiv 1.3 \times 10^{38} (M_{pbh}/1 M_\odot) \text{ erg s}^{-1}$. The ra-

diative efficiency ϵ determines the accretion luminosity for a given accretion rate: $L_{bol} = \epsilon \dot{M}_b c^2$. Thus, defining the Eddington accretion rate as $\dot{M}_{Ed} \equiv L_{Ed}/c^2 = 1.44 \times 10^{17} (M_{pbh}/M_\odot) \text{ g s}^{-1}$ and the dimensionless accretion rate as $\dot{m} \equiv \dot{M}_b/\dot{M}_{Ed}$ we have $l = \epsilon \dot{m}$.

The dimensionless Bondi-Hoyle accretion rate for a PBH without a dark halo is:

$$\dot{m} = (1.8 \times 10^{-3} \lambda) \left(\frac{1+z}{1000} \right)^3 \left(\frac{M_{pbh}}{1 M_\odot} \right) \left(\frac{v_{eff}}{5.74 \text{ km s}^{-1}} \right)^{-3}. \quad (22)$$

This equation is valid only if PBH constitute all the dark matter: $f_{pbh} = \Omega_{pbh}/\Omega_{dm} = 1$. If the accreting object is a point mass (*i.e.*, a “naked” PBH), λ depends only on the value of the dimensionless gas viscosity $\hat{\beta} = \beta^{eff} r_B/c_s$: if $\hat{\beta} \ll 1$ we find $\lambda \sim 1$ and if $\hat{\beta} \gg 1$ we have $\lambda \sim 1/\hat{\beta}$. The fit to the accretion eigenvalue for an isothermal gas is given by the formula (see Paper II),

$$\lambda = \exp \left(\frac{9/2}{3 + \hat{\beta}^{0.75}} \right) x_{cr}^2 \quad (23)$$

where the dimensionless sonic radius ($x_{cr} \equiv r_{rc}/r_B$) is $x_{cr} = [-1 + (1 + \hat{\beta})^{1/2}]/\hat{\beta}$. The effective gas viscosity, $\beta^{eff} = \beta + H$, is the sum of two terms. The first term, due to Compton drag, is $\beta(z) = 2.06 \times 10^{-23} x_e (1+z)^4 \text{ s}^{-1}$, and the second, due to the cosmic expansion, is the Hubble parameter $H(z)$. It is easier to understand the physical meaning of the dimensionless viscosity due to the Hubble expansion in terms of the recession velocity of the gas due to the Hubble flow at the Bondi radius: $v_H \sim r_B H(z)$. As expected, if $v_H/c_s = \hat{\beta}_{Hubble} \ll 1$ we can neglect the cosmic expansion. The dimensionless viscosity depends on the redshift, the mass of the PBH and the temperature and ionization fraction of the cosmic

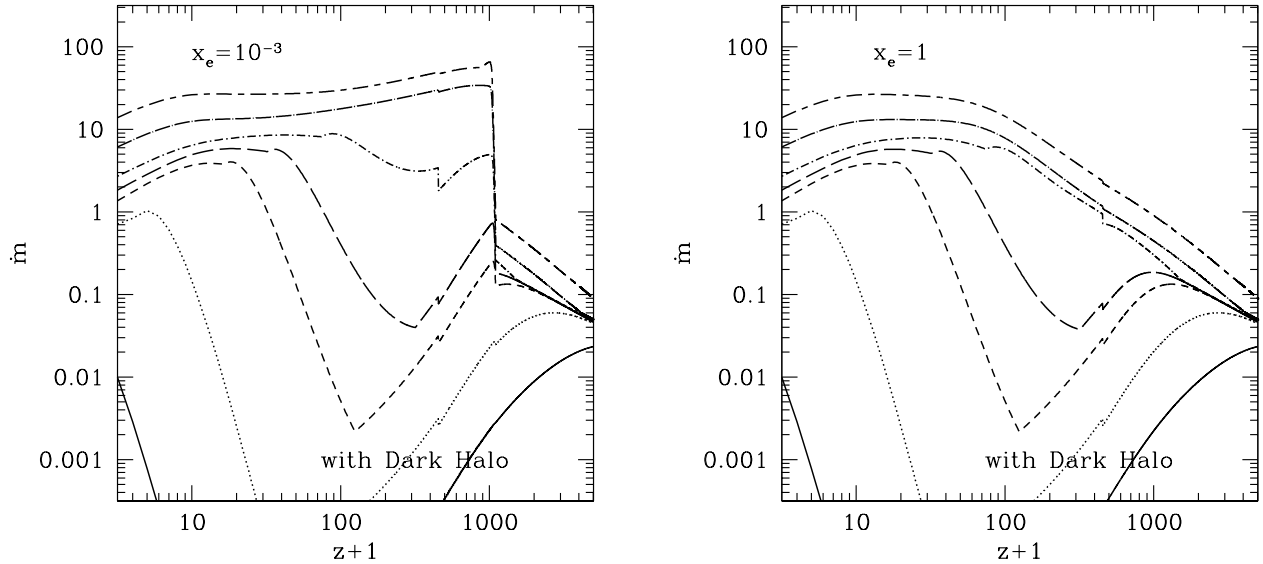


FIG. 4.— Same as in Fig. 3 but including the growth of the dark halo surrounding the PBH ($\alpha = 2.25$ and $\phi_i = 3$). The curves from bottom to top refers to $M_{pbh} = 1, 10, 100, 300, 10^3, 10^4, 10^5 M_\odot$.

gas:

$$\hat{\beta} = \left(\frac{M_{pbh}}{10^4 M_\odot} \right) \left(\frac{z+1}{1000} \right)^{3/2} \left(\frac{c_s}{5.74 \text{ km s}^{-1}} \right)^{-3} \times \left[0.257 + 1.45 \left(\frac{x_e}{0.01} \right) \left(\frac{z+1}{1000} \right)^{5/2} \right]. \quad (24)$$

Fig. 3 shows the accretion rate \dot{m} from equations (22)-(23) as a function of redshift. The curves from bottom to top refer to $M_{pbh} = 1, 10, 100, 10^3, 10^4, 10^5 M_\odot$. We assume a gas with constant electron fraction $x_e = 10^{-3}$ after recombination in the left panel and $x_e = 10^{-1}$ in the right panel. Thermal feedback is neglected and recombination is instantaneous.

If $f_{pbh} < 1$ we need to consider the effect of a growing dark matter halo with mass $M_h(z) = \phi_i M_{pbh} [(1+z)/1000]^{-1}$. For $\phi_i = 3$ we find

$$\dot{m} = (0.016\lambda) \left(\frac{1+z}{1000} \right) \left(\frac{M_{pbh}}{1M_\odot} \right) \left(\frac{v_{eff}}{5.74 \text{ km s}^{-1}} \right)^{-3}. \quad (25)$$

In the simulations presented in § 5, we impose that the dark halo stops growing when all the available dark matter has been accreted; *i.e.*, when $f_{pbh} \phi_i [(1+z)/1000]^{-1} = 1$. The gas accretion onto an extended dark halo of mass M_h and power-law density profile with logarithmic slope $2 < \alpha < 3$ is related to the one for a point mass (with $M_{pbh} = M_h$) by the following scaling relationships (see Paper II):

$$\hat{\beta}^{(h)} \equiv \chi^{\frac{p}{1-p}} \hat{\beta}, \quad \lambda^{(h)} \equiv \Upsilon^{\frac{p}{1-p}} \lambda, \quad r_{cr}^{(h)} \approx \left(\frac{\chi}{2} \right)^{\frac{p}{1-p}} r_{cr}. \quad (26)$$

where $\chi = r_B/r_h < 2$, $p = 3 - \alpha$, and

$$\Upsilon = \left(1 + 10\hat{\beta}^{(h)} \right)^{\frac{1}{10}} \exp(2 - \chi) \left(\frac{\chi}{2} \right)^2. \quad (27)$$

When the Bondi radius r_B is larger than twice the radius of the dark halo ($\chi \geq 2$), the dark halo behaves the same

as a point mass in terms of accretion rate, sonic radius and dimensionless viscosity. The numerical value of χ is

$$\chi = 0.22 \left(\frac{M_h}{1M_\odot} \right)^{\frac{2}{3}} \left(\frac{1+z}{1000} \right) \left(\frac{c_s}{1 \text{ km s}^{-1}} \right)^{-2}. \quad (28)$$

We adopt the parameters $\alpha = 2.25$, $\phi_i = 3$ and r_h given in equation (8), valid for a quasi-spherical dark halo in which the dark matter does not fall directly onto the PBH. Figure 4 shows the accretion rate, \dot{m} , from equations (25)-(26) as a function of redshift, with the curves representing the same masses as Fig. 3 with the same simplifying assumptions going into the simulation.

3.6. Accretion luminosity

The radiative efficiency ϵ of accreting black holes is known to depend on the accretion rate \dot{m} and the geometry of the accretion flow. Observations and theoretical models suggest that the radiative efficiency approaches a constant value $\epsilon \sim 0.1$ for accretion rates $\dot{m} \gtrsim 1$. If the accretion rate is $\dot{m} \lesssim 1$ the radiative efficiency is smaller by a factor $\epsilon \propto \dot{m}$ (*e.g.*, Park & Ostriker 2001). Depending on the angular momentum of accreted material, a thick disk may form. Otherwise the accretion geometry is spherical. The later case is the most conservative as the accretion efficiency is minimum. In addition, this case is appropriate for most PBH masses which have $\dot{m} < 1$ (see § 3.3). We consider the following accretion regimes:

Thin disk: If $\dot{m} > 1$ we assume that the gas accreted by the PBH forms a thin accretion disk and has radiative efficiency $\epsilon = 0.1$. We assume that the bolometric luminosity cannot exceed the Eddington limit and that, due to complex feedback effects that we do not attempt to model here, the PBHs accrete near the Eddington limit only for a fraction of time f_{duty} . Observations of AGN at redshifts $z < 3$ show that typically f_{duty} is about three percent (Shapley et al. 2003, *e.g.*). However, for PBHs, the duty cycle can be substantially different as the nature of the feedback mechanisms which regulate the cycle are

not well understood. We let f_{duty} be a free parameter and we show that the limits on the PBH abundance scale linearly with it. In summary,

$$l = f_{pbh} \times \min(0.1\dot{m}, 1) \quad \text{if } \dot{m} > 1. \quad (29)$$

Figures 3-4 show that this choice of the radiative efficiency is appropriate for PBHs with masses $M_{pbh} \gtrsim 100 M_{\odot}$. The spectrum of the radiation emitted by the accreting material depends on the accretion geometry, accretion rate, and the mass of the black hole. For a thin disk, any given radius emits black body radiation with different emission temperature (multicolor disk). The disk is hot in the inner parts and colder in the outer parts. The maximum temperature of the disk depends on the black hole mass: $T_{max} \propto M_{pbh}^{-1/4} \dot{m}$. Beyond photon energies kT_{max} the emission is dominated by non-thermal radiation produced by a diffuse hot corona around the accretion disk. The spectrum of the non-thermal component is a power law of the form $\nu L_{\nu} \propto \nu^{-\beta}$ with $\beta \sim 1.5$. Guided by observations we model the spectrum as a double power-law with a break at energies $h\nu = kT_{max}$ with slope $\beta = 0.3$ at low energy and $\beta = 1.6$ at high energy.

Spherical accretion or ADAF: If $\dot{m} < 1$ the accretion efficiency depends on the flow geometry. If the infall is quasi-spherical the radiative efficiency is minimal. The dominant emission mechanism is thermal bremsstrahlung. Most of the radiation will originate from the region just outside the event horizon. For the case of accretion from a neutral HI gas, including relativistic effects, the efficiency for conversion of rest-mass energy into radiation is $\epsilon = 0.011\dot{m}$ (Shapiro 1973a,b). Hence,

$$l = 0.011\dot{m}^2 \quad \text{if } \dot{m} < 1 \text{ (spherical accretion)}. \quad (30)$$

The spectrum is well approximated by a power law of the form $\nu L_{\nu} \propto \nu^{0.5}$ at $\nu > 13.6$ eV and has an exponential cut-off at $\nu \sim 5 \times 10^5$ eV (Shapiro 1973a). This case gives the most conservative estimate of the effect of PBHs on the cosmic ionization history. In addition some authors have found that when the effects of magnetic field and cosmic rays are included in the calculations, the radiative efficiency can be larger than the $0.01\dot{m}$ assumed in our fiducial case (Meszaros 1975b).

If the gas has non-negligible angular momentum, an advection dominated accretion flow (ADAF) may form (Narayan & Yi 1995). In this case the radiative efficiency is a factor of ten larger: $\epsilon = 0.1\dot{m}$. Hence, $l = 0.1\dot{m}^2$. This case is not particularly relevant for our study as we have seen in § 3.3 that only PBHs with masses $> 1000 M_{\odot}$ can form accretion disks and typically for these masses we find $\dot{m} > 1$.

3.6.1. Is the emerging radiation trapped by the accreting gas?

Assuming spherical accretion and negligible pressure with respect to the gravitational potential, the gas falling onto PBHs acquires a velocity that approaches the free fall velocity near the black hole.¹ From mass conservation it follows that the gas density profile is $\rho_g \propto r^{-1.5}$

¹ For realistic cases in which the angular momentum of accreting gas is important we refer to previous well known studies of hot optically thin accretion flows (Shapiro et al. 1976; Narayan & Yi 1995).

in the inner parts. Hence, the gas column density $N_g \propto r^{-1/2}$ diverges for radii $r \rightarrow 0$ and so does the Compton scattering optical depth for outgoing radiation.

We checked whether the accreting gas may become opaque to Compton scattering. In this case, the infalling gas would trap the emerging X-ray photons (which are mostly emitted near the black hole horizon) or the X-ray photons may be reprocessed into lower energy photons. The optical depth for emerging radiation emitted at a distance $r_{min} = \alpha R_{Sch}$ from the black hole,

$$\tau_e = \frac{\sigma_T}{m_p} \int_{r_{min}}^{r_{max}} \rho_g dr = \frac{\dot{m}}{\alpha^{1/2}}, \quad (31)$$

where $\alpha \geq 1$ is the distance in units of the black hole Schwarzschild radius and where we have assumed $r_{max} \gg r_{min}$. Hence, for any value of the accretion rate smaller than $\dot{m} \sim \alpha^{1/2} \sim 1$ the gas is optically thin to Compton scattering. Since we assume that PBHs with $\dot{m} > 1$ form an thin accretion disk, we can safely neglect trapping of radiation emitted near the black hole in all the models we consider. Similar calculations show that the gas accreting onto PBHs is transparent (to Compton scattering) to external background radiation.

4. FEEDBACK PROCESSES

Gas accretion onto PBHs produces radiation that heats and ionizes the IGM, thus raising its temperature above the value given in equation (5). X-ray photons, having a mean free path larger than the mean distance between the sources, tend to build up a uniform radiation background that increases the ionization fraction of the gas and heats the IGM. The UV radiation, on the other hand, is absorbed not very far from the emitting sources, so UV photons produce spheres of fully ionized hydrogen around each PBH. These processes introduce global and local feedback effects which may alter the accretion rate. Here we describe these effects and comment on their importance for the accretion calculation.

4.1. Global Feedback

We use a semianalytic code, described in detail in (Ricotti & Ostriker 2004) and based on (Chiu & Ostriker 2000), to follow the chemical, ionization and thermal history of the IGM from recombination to the redshift of the formation of the first galaxies. We consider a gas of primordial composition and include H₂ formation/destruction processes. Although the code includes a stellar reionization and galaxy formation formalism, in the present paper we focus on the cosmic epochs preceding the formation of the first galaxies. In addition to the emission from PBHs we include the contribution from the CMB radiation background that gives us a redshift of recombination $z_{rec} \sim 1000$, in good agreement with observations.

The thermal feedback by the X-ray background is calculated self-consistently: the temperature and ionization of the cosmic gas is determined by the luminosity of PBHs, and the PBH accretion rate is a function of the gas temperature and ionization. The thermal and chemical history is calculated iteratively until the solution converges. The total emissivity per unit mass from accretion onto PBHs is proportional to $l f_{pbh}$. At $z < 30$, when the age of the universe is $t \sim 10^7$ yr, accretion onto

PBHs stops due to their peculiar velocities. Even if we assume that PBHs accrete at the Eddington rate before $z = 30$, the accretion time scale $t_{Salp} = 4.4 \times 10^8$ yr is much larger than the age of the universe at this redshift. Hence, the growth of PBHs by gas accretion is negligible.

4.2. Local Feedback and Duty Cycle

In addition to tracking the X-ray background, the semianalytic code simulates the evolution of the Strömgren spheres produced by UV radiation. These ionized bubbles have a small volume filling factor and thus a negligible effect on the ionization history. Nevertheless, the gas is ionized and heated by UV radiation within the H II regions, leading to local feedback effects that may reduce the gas accretion rate.

Local feedback may reduce the gas accretion rate if: i) the radius of the H II region exceeds the Bondi radius ($r_{HII} > r_B$), and ii) if the gas temperature inside the H II region is higher than the temperature outside. Although this is always the case at low redshifts, at $z > 30$ the Compton coupling between the free electrons inside the H II regions and the CMB radiation is very effective in keeping the gas temperature near the CMB temperature.

If the final size of the H II region is larger than the Bondi radius ($r_{HII}/r_B > 1$) and the temperature inside the H II region is much larger than that outside, then the gas accretion rate may stop or decrease. For simplicity, let's consider the most extreme scenario, in which when $r_{HII}/r_B \geq 1$, the luminosity becomes negligible and the H II region recombines. With this assumption the time averaged luminosity can be estimated to be

$$\langle l \rangle_t = \frac{l}{1 + t_{off}/t_{on}} = \frac{l}{1 + (r_{HII}/r_B)^{1/3}} = f_{duty}l, \quad (32)$$

where $t_{off} = t_{rec,H}$ is the H I recombination timescale and $t_{on} = t_{rec,H}(r_B/r_{HII})^{1/3}$ is the timescale it takes for the ionization front to reach the Bondi radius r_B . Thus, it follows $t_{off}/t_{on} = (r_{HII}/r_B)^{1/3}$. Equation (32) gives a rough estimate of the duty cycle produced by local feedback.

4.2.1. Temperature structure of the H II region

We have performed time-dependent 1D radiative transfer simulations of the H II regions around PBHs to estimate r_{HII} and the temperature T_{HII} inside the Strömgren radius. The basic results can be also derived analytically. The radius of the Strömgren sphere around a PBH of mass M_{pbh} at the center of a spherical gas cloud with density profile $n_{gas} = n_{H0}(r/r_0)^\gamma$, where $n_{H0}(z)$ is the mean cosmic density of the gas, is

$$r_{HII} = (0.77 \text{ pc}) \left(\frac{S_0}{f_\gamma} \right)^{1/3} \left(\frac{1+z}{1000} \right)^{-2}, \quad (33)$$

where $f_\gamma = 1/3$ for $\gamma = 0$ (*i.e.*, assuming gas at uniform density) or $f_\gamma \sim \ln(r_0/r_{min}) \sim 10$ assuming a free falling gas that becomes collisionally ionized at r_{min} (*i.e.*, we adopt $\gamma = -1.5$ and $r_0/r_{min} \sim 10^4$). We have defined the quantities

$$S_0 \equiv (6 \times 10^{-3})l \left(\frac{M_{pbh}}{1 M_\odot} \right) \left(\frac{X}{100} \right)^{-1}, \quad (34)$$

the number of ionizing photons emitted per second in units of 10^{49} photons s^{-1} , and

$$X \equiv \left(\frac{h\nu_0}{L_{bol}} \int_{\nu_0}^{\infty} \frac{L_\nu}{h\nu} d\nu \right)^{-1} \quad (35)$$

the mean energy of the emitted photons in Rydberg units ($h\nu_0 = 13.6$ eV). Assuming a power-law spectrum with index $\beta = 0.5$ in the frequency interval $13.6 < \nu < 5 \times 10^5$ eV, appropriate for spherical accretion, we find $X \sim 192$. For thin disk accretion we find $X = \beta/(\beta - 1) \sim 3$ for $\beta = 1.5$. In order to estimate the value of the Strömgren radius we assumed an H I recombination coefficient $\alpha = 1.28 \times 10^{-12} \text{ cm}^{-3} \text{ s}^{-1}$, appropriate for a gas at $T \sim 2,000$ K. This temperature is typical for the gas inside an H II region at $z \sim 500$.

We now estimate the temperature inside the H II region assuming that the dominant gas heating is H I photoionization and the dominant cooling is Compton cooling. In a uniform density gas in ionization and thermal equilibrium the temperature inside the H II region is constant. At equilibrium the ionization rate per hydrogen atom equals the recombination rate: $t_{ion} = t_{rec,H} \sim (124 \text{ yr})[(1+z)/1000]^{-3}$ and the heating rate is $\langle h\nu \rangle / t_{ion}$, where $\langle h\nu \rangle \sim 0.365 \text{ eV}/(\beta + 2)$ is the mean photon energy deposited into the gas per hydrogen atom. Neglecting Compton heating, which is only important in a small volume around the black hole, a fraction $C \sim 0.0268/(\beta + 2)X$ of the radiation emitted by the black hole is deposited as heat inside the H II region. If we assume that the heating rate equals the Compton cooling rate $k(T_{HII} - T_{CMB})/t_{Comp}$, where $t_{Comp} \sim (0.76 \text{ yr})[(1+z)/1000]^{-4}$ we find

$$\frac{T_{HII}}{T_{CMB}} \approx 1 + \frac{0.36}{\beta + 2} \left(\frac{1+z}{1000} \right)^{-2}. \quad (36)$$

Thus, for spherical accretion with $\beta = 0.5$ (disk accretion with $\beta = 1.5$) the temperature inside the H II regions at $z \sim 500$ is only 56% (41%) higher than the temperature outside, which is roughly equal to the CMB temperature $T_{CMB} \approx 1375$. We conclude that at high redshift, even if the Bondi radius is smaller than the Strömgren radius, the increase of the IGM temperature due to local feedback is negligible. Hence, we can neglect the local contribution to thermal feedback (from UV photos) with respect to the global thermal feedback from X-ray heating, that is always included self-consistently (see § 4.1)

More sophisticated radiative transfer simulations confirm the results of the analytical calculations of r_{HII} and T_{HII} . In Fig. 5 we show the time evolution of the temperature profile inside an H II region around a PBH with $S_0 = 10^{52} \text{ s}^{-1}$ at $z \sim 500$. The 1D radiative transfer code used to produce the temperature plots is described in detail in Ricotti et al. (2001). In addition, in the present simulation we have also included Compton heating from X-rays emitted near the PBH. The increase of the gas temperature at small radii evident in Fig. 5, $T \propto r^{-2}$, is produced by Compton heating. We estimate that Compton heating becomes dominant over photoionization heating at radii

$$r < \left(\frac{X}{\langle h\nu \rangle} \right)^{1/2} \left(\frac{kT}{m_e c^2} \right)^{1/2} (\sigma_T S_0 t_{rec,H})^{1/2}$$

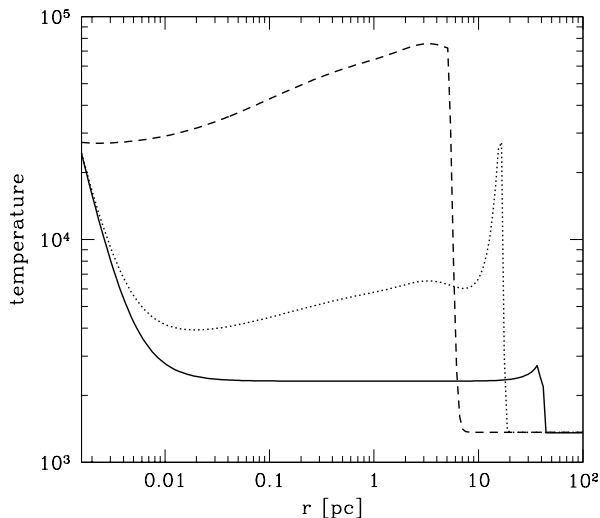


FIG. 5.— (a) Temperature structure of the H II region around a PBH at $z = 500$ emitting $S_0 = 10^{52}$ ionizing photons per second. The curves show the temperature profile after 2 yr (dashed), 100 yr (dotted) and 4600 yr (solid) after the source turns on. The source spectrum is one appropriate for spherical accretion onto a black hole, with log-slope $\beta = 0.5$.

$$\approx (0.01 \text{ pc}) S_{0,49}^{\frac{1}{2}} \left(\frac{1+z}{1000} \right)^{-\frac{3}{2}}. \quad (37)$$

After a time-dependent phase during which the H II region reaches its Strömgen radius, the temperature inside the H II region decreases to a constant value $T_{HII} \sim 2,100$ K, about 56% higher than the temperature outside the H II regions, in agreement with the analytical estimate. We have verified that the temperature T_{HII} is independent of the source luminosity and depends on β and the redshift according to equation (36).

4.2.2. Strömgen vs Bondi radii

Let's now estimate the ratio r_{HII}/r_B , which, along with the H II region gas temperature, determines whether local feedback will reduce the gas accretion rate. From equation (3) and equation (33) with $f_\gamma = 10$ we find

$$\frac{r_{HII}}{r_B} \sim 3 \times 10^3 \left(\frac{l}{X} \right)^{\frac{1}{3}} \left(\frac{M_{pbh}}{1 M_\odot} \right)^{-\frac{2}{3}} \times \left(\frac{1+z}{1000} \right)^{-2} \left(\frac{v_{eff}}{5.7 \text{ km s}^{-1}} \right)^2 \quad (38)$$

for “naked” PBHs. If we include the growth of an extended dark halo, r_{HII}/r_B decreases by a factor $0.3[(1+z)/1000]$ at $z < 1000$. We shall consider two cases for the accretion luminosity: Case A, appropriate for small accretion rates $\dot{m} < 1$ and Case B, appropriate for $\dot{m} \sim 1 - 10$ (see § 3.6).

Case A: $l \propto \dot{m}^2$.

The case $l \propto \dot{m}^2$ is the most interesting because is the most likely to occur for PBHs and because the ratio r_{HII}/r_B is independent of the gas effective velocity v_{eff} and PBH mass. Indeed, $r_{HII} \propto l^{2/3} \propto v_{eff}^{-2}$ and $r_B \propto v_{eff}^{-2}$. Assuming $\epsilon = 0.01$ (spherical accretion) we

find that the ratio

$$\frac{r_{HII}}{r_B} \sim 2 \left(\frac{X}{200} \right)^{-\frac{1}{3}} \quad (39)$$

is a constant of order of unity for a “naked” PBH with mass $M_{pbh} < M_{cr} \sim 10^4 M_\odot$ and $\dot{m} < 1$. For PBHs more massive than M_{cr} , the constant is smaller by a factor $(M_{pbh}/M_{cr})^{2/3}$, thus local radiative feedback can be safely neglected because $r_{HII} < r_B$. Including the growth of the dark halo around PBHs we find:

$$\frac{r_{HII}}{r_B} = 0.66 \left(\frac{1+z}{1000} \right) \left(\frac{X}{200} \right)^{-\frac{1}{3}} < 1, \quad (40)$$

valid only at redshifts $z \gtrsim 100$. At lower redshifts, r_{HII}/r_B increases with respect to the estimate in equation (40) but its value remains on order unity or smaller for $\dot{m} < 1$.

Case B: $l \propto \dot{m}$.

This case applies to the case of relatively massive PBHs with typical masses $> 10^3 M_\odot$ that have $1 < \dot{m} < 10$ or $0.1 < l < 1$. It is sufficient to consider the case of a PBH clothed in its dark halo. We find

$$\frac{r_{HII}}{r_B} \sim 4 \left(\frac{M_{pbh}}{10^4 M_\odot} \right)^{-2/3} \left(\frac{X}{3} \right)^{-1/3}. \quad (41)$$

Thus, $r_{HII} < r_B$ for $M_{pbh} \gtrsim 10^5 M_\odot$. Also in this case we can neglect local feedback with the exception of the mass range $10^3 - 10^5 M_\odot$ where local thermal feedback may reduce accretion by a factor of a few (from equation (32) we obtain a reduction $f_{duty} \sim 30\%$ for $M_{pbh} \sim 10^3 M_\odot$).

In summary, the local feedback due to the formation of an H II region around the PBH can be neglected in most cases. At high redshift the temperature inside the H II regions is only a few tens of a percent higher than the temperature outside (see equation [36]), thus even if the Bondi radius is smaller than the Strömgen radius, the reduction of the accretion rate due to thermal feedback is negligible. At lower redshifts ($z < 100$) the temperature inside H II regions is larger than the temperature outside but we found that the Strömgen radius is typically smaller than the Bondi radius.

The only exceptions are massive PBHs with $10^3 M_\odot < M_{pbh} < 10^5 M_\odot$ for which we estimate $f_{duty} \lesssim 30\%$. For this case, since $r_{HII} > r_B$, we need to also assume that the gas is fully ionized at the Bondi radius. Hence, in addition to thermal feedback, the ionized gas inside the H II region increases the gas viscosity due to Compton drag. Compton drag is negligible at $z < 100$ (see Figs. 3-4) but reduces the accretion rate at $z > 100$ when, instead, thermal feedback is negligible.

5. SIMULATING THE COSMIC IONIZATION

We simulate the ionization, chemical and thermal history of the universe after recombination using a modification of the semianalytic code discussed in detail in Ricotti & Ostriker (2004). The original code is tailored to simulate UV and X-ray reionization from high redshift galaxies at $z < 30$. Here we do not include any ionizing source other than PBHs. In order to simulate standard recombination properly we model the redshifted CMB black body radiation including the effect of Thompson

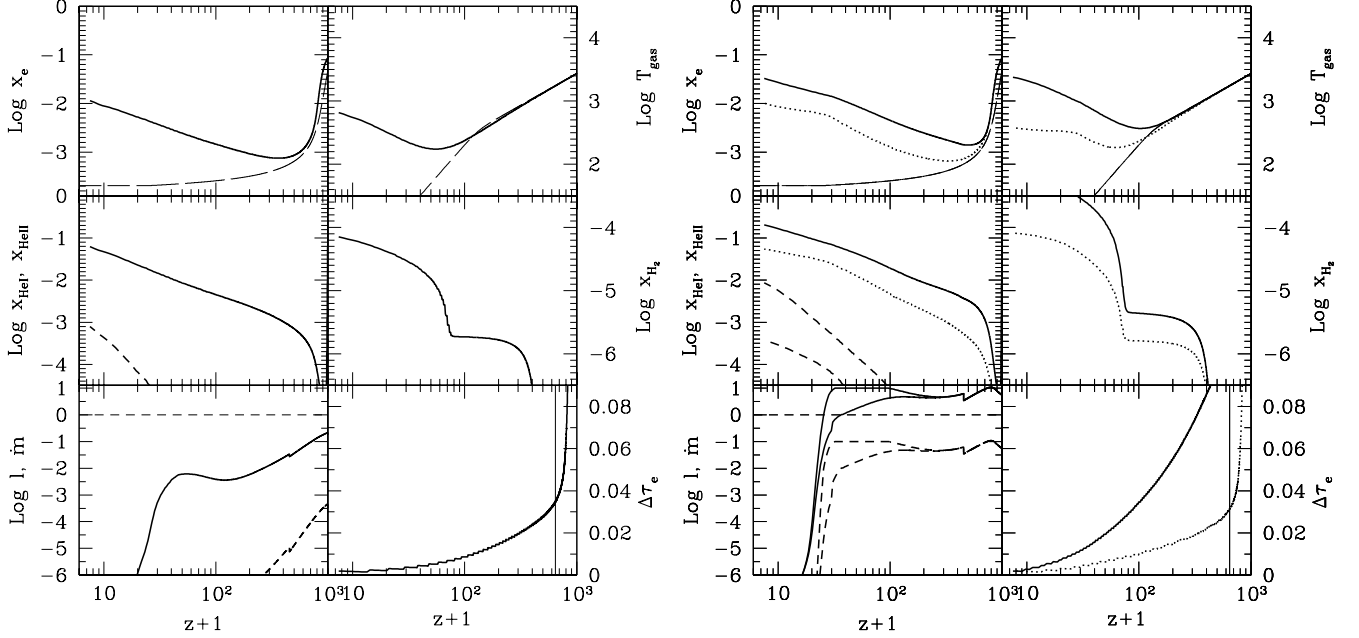


FIG. 6.— *Left.* Simulation of early ionization by PBHs with mass $M_{\text{pbh}} = 100 M_{\odot}$ and abundance $f_{\text{pbh}} = 10^{-4}$. The panels show: (a) the ionization fraction x_e (the dashed line shows the recombination history without PBHs); (b) the temperature (the dashed line shows the thermal history without PBHs); (c) the He ionization fraction; (d) the H_2 abundance; (e) the accretion rate, \dot{m} (solid curve) and luminosity l (dashed curve); (f) the optical depth to Thompson scattering τ_e . *Right.* Same as in the left panel but for $M_{\text{pbh}} = 1000 M_{\odot}$ and $f_{\text{pbh}} = 10^{-6}$ (solid curves) and $f_{\text{pbh}} = 10^{-7}$ (dotted curves).

opacity. We test the recombination history calculation in the absence of PBHs against a widely used code RECFAST (Seager et al. 1999). We can reproduce the recombination history at redshifts $z < 900$ (when $x_e < 0.1$) with accuracy of a few percent. Using the equations derived in this work we model the UV and X-ray emission from accreting PBHs including feedback effects, the secondary ionization due to fast photo-electrons, and Compton heating/cooling, and we solve the chemical network for a gas of primordial composition (*e.g.*, molecular hydrogen formation/dissociation). We run a grid of models with a range of PBH masses spanning several orders of magnitude, between $10^{-3} M_{\odot}$ to $10^8 M_{\odot}$.

For the sake of simplicity, throughout the rest of the paper we consider the effects of a population of equal mass PBHs which account for a fraction f_{pbh} of the dark matter. The results can be used to estimate the effect of an arbitrary PBH mass function by integrating the optical depth $d\tau_e(M)$ in each mass bin with weight function $(df_{\text{pbh}}/dM)^{1/2}$. See below for an explanation of the choice of the weighting function. Special care should be taken in excluding from the integration PBHs which are sufficiently small to be part of the dark halos of more massive PBHs. In addition we need to check that the proper velocities of small PBHs, due to their interaction with more massive ones, is negligible (*i.e.*, subsonic). Fitting formulas for τ_e as a function of M_{pbh} and f_{pbh} are provided at the end of this section.

Independently of the radiation emitted by the gas falling directly onto the PBHs, gas inflow onto the PBH can produce shocks and collisional ionization. For the idealized case of an isothermal gas the sonic point is located at $0.5r_B$, where r_B is the Bondi radius. At this point a shock develops that ionizes the gas, even if the temperature remains below 10,000 K due to Comp-

ton cooling and molecular hydrogen cooling. The volume filling factor of the collisionally ionized gas is $f_V \sim n_{\text{pbh}}(r_B/2)^3$, where n_{pbh} is the PBH physical number density. Assuming that a fraction of the IGM f_V is fully ionized and the rest of the cosmic gas is neutral we have a volume-weighted ionization fraction due to shocks: $\langle x_e \rangle_V \approx 10^{-11} f_{\text{pbh}} (M_{\text{pbh}}/1 M_{\odot})^2$. This effect is negligible for any PBH mass assuming values of f_{pbh} allowed by observational constraints.

Examples of simulations with $M_{\text{pbh}} = 100 M_{\odot}$ and $1000 M_{\odot}$ are shown in Fig. 6. Here, we describe simulations in models that are consistent with FIRAS and WMAP3 data. In these models the contribution of PBHs to the total optical depth to Thompson scattering typically does not exceed $\Delta\tau_e \sim 0.03 - 0.04$ at 68% confidence level and $\Delta\tau_e \sim 0.07 - 0.09$ at 95% confidence level. The contribution is uncorrelated with the value of τ_e produced by ionization sources in high redshift galaxies (at $z < 30$) which is $\tau_e = 0.09 \pm 0.03$ (see § 6).

The mean electron fraction increases approximately as $x_e \propto (z+1)^{-1}$ from $x_e \sim 10^{-3}$ at $z \sim 900$ to values close to $x_e \sim 10^{-1} - 10^{-2}$ at $z \sim 10$. Hence, the viscous effect of Compton drag can be neglected after recombination. The main contribution to the partial ionization of the cosmic gas after recombination is from X-ray emission at redshifts $z > 100$. At smaller redshifts, due to the rapid decline of the accretion rate onto PBHs, the ionization fraction keeps increasing slowly, due to redshifted X-ray background photons (Ricotti & Ostriker 2004). The gas temperature is approximately equal to the CMB temperature at $z > 200$ and ranges between 100 K to 1000 K afterwards. The He II ionization fraction becomes 1–10% and the molecular abundance $x_{\text{H}_2} \sim 10^{-4} - 10^{-5}$ after redshift $z \sim 100$. The molecular abundance is 10–100 times larger than the standard value, $x_{\text{H}_2} \sim 10^{-6}$, ob-

tained neglecting PBHs. Depending on the mass of PBHs we encounter different regimes for the accretion.

1) $1 M_\odot < M_{pbh} < 30 M_\odot$: The dark halo has negligible effect on the accretion rate. The accretion is spherical and the luminosity $l \propto \dot{m}^2$. Global feedback effects are negligible.

2) $30 M_\odot < M_{pbh} < 300 M_\odot$: The dark halo increases the accretion rate onto PBHs, mostly at redshifts $z < 100$. The accretion is spherical and the luminosity $l \propto \dot{m}^2$. Global feedback effects are important in reducing the accretion rate at $z < 100$.

3) $300 M_\odot < M_{pbh} < 3000 M_\odot$: The dark halo increases the accretion rate onto PBHs at all redshifts. The accretion rate is large ($\dot{m} \gtrsim 1$), thus a thin disk may form and the luminosity is $l \propto f_{duty} \dot{m}$. Global feedback effects moderately reduce the accretion rate.

4) $M_{pbh} > 3000 M_\odot$: The dark halo increases the accretion rate onto PBHs at all redshifts. For masses $> 5 \times 10^4 M_\odot$, the Hubble expansion becomes important and the Bondi solutions transition to self-similar infall solutions (see Paper II). PBHs accrete at the Eddington rate with a duty cycle f_{duty} . Global feedback effects do not reduce the accretion rate significantly for values $\Delta\tau_e \lesssim 0.05$, compatible with WMAP3 (see § 6).

The qualitative dependence of $x_e(z)$ and $\tau_e(z)$, on the mass and abundance of PBHs can be understood assuming ionization equilibrium. For $x_e(z) \ll 1$ and neglecting the temperature dependence of the recombination coefficient we have $x_e(z)^2 \propto l(z, M_{pbh}) f_{pbh}$. For PBHs with masses smaller than $M_{pbh} \sim 100 M_\odot$ we have $\dot{m} < 1$ and $l \propto M_{pbh}^2$. Hence, $\tau_e \propto x_e \propto M_{pbh} f_{pbh}^{1/2}$. If the mass of the PBH is $\gtrsim 100 M_\odot$ the accretion rate is typically $\dot{m} > 1$, $l \propto M_{pbh}$ and $\tau_e \propto x_e \propto (M_{pbh} f_{duty} f_{pbh})^{1/2}$. Finally, if $M_{pbh} \gtrsim 1000 M_\odot$ we have $\dot{m} \geq 10$, PBHs accrete nearly at the Eddington limit and $\tau_e \propto x_e \propto (f_{duty} f_{pbh})^{1/2}$ is independent of the PBH mass. To first order, the value of $\Delta\tau_e$ produced by PBHs of mass M_{pbh} and abundance f_{pbh} can be parameterized as follows:

$$\Delta\tau_e \approx \begin{cases} 0.05 \left(\frac{M_{pbh}}{1 M_\odot} \right) f_{pbh}^{1/2} & \text{if } M_{pbh} < 100 M_\odot, \\ 0.1 \left(\frac{M_{pbh}}{1 M_\odot} \right) (f_{duty} f_{pbh})^{1/2} & \text{if } 10^2 < \frac{M_{pbh}}{1 M_\odot} < 10^3, \\ 10^5 (f_{duty} f_{pbh})^{1/2} & \text{if } M_{pbh} > 10^3 M_\odot. \end{cases} \quad (42)$$

The fit is derived from a grid of simulations with $\Delta\tau_e < 0.2$ and is not accurate for large values of $\Delta\tau_e$ due to feedback and saturation effects.

6. EFFECTS OF PBHS ON THE CMB SPECTRUM AND ANISOTROPIES

6.1. Temperature and Polarization Anisotropies

In § 5 we have shown that a signature of the existence of PBHs is the modification of the cosmic recombination history. It is possible to construct models with $\tau_e \sim 1$ due to the large residual fractional ionization of the cosmic gas after recombination produced by X-ray ionization. Of course, such models are ruled out by CMB observations. The WMAP3 constraint on τ_e is $\tau_e \sim 0.09 \pm 0.03$. This limit on τ_e assumes that the intergalactic medium becomes partially or fully ionized by stars and/or black holes starting at redshift $z \lesssim 30$. As illustrated in Fig. 7, the partial ionization from PBHs and the ionization from

high redshift galaxies forming at $z < 30$ produce very different signatures on the CMB polarization anisotropies. PBHs affect small angular scales with $l \gtrsim 10$, while radiation emitted by high redshift galaxies affect larger scales with $l < 10$. Hence, PBHs do not contribute significantly to the value $\tau_e = 0.09$ quoted by the WMAP3 team, which must be produced by ionization sources other than PBHs.

In order to constrain models which allow for the existence of PBHs we include an additional cosmological parameter describing the deviation from the standard recombination history calculated using RECFAST (Seager et al. 1999). We have modified the publicly available codes CAMCMB and COSMOMC (Lewis & Bridle 2002) to include an additional degree of freedom. The redshift dependence of the ionization history after recombination depends weakly on the mass of PBHs for values of $\Delta\tau_e \lesssim 0.1$. We modify the recombination history $x_{e,rec}(z)$ given by RECFAST as follows:

$$x_e(z) = x_{e,rec}(z) + \min \left[x_{e0} \left(\frac{1+z}{1000} \right)^{-1}, 0.1 \right], \quad (43)$$

The free parameter x_{e0} is the ionization fraction at $z = 1000$. The ionization fraction increases proportionally to the scale parameter after recombination and is constant at later times. In addition, we model the instantaneous reionization at $z = z_{rei}$ produced by galactic sources. We will show that the effect on the CMB polarization anisotropies of PBHs and other ionizing sources are uncorrelated.

Using the Markov Chain Monte-Carlo code COSMOMC with WMAP3 data we find 1σ and 2σ marginalized confidence limits for the new free parameter: $x_{e0} < 2 \times 10^{-4}$ (68% CF) and $x_{e0} < 4.2 \times 10^{-4}$ (95% CF). These upper limits on the fractional ionization correspond to upper limits on $\Delta\tau_e = \tau_e - \tau_{e,rei}$ of 0.05 (68% CF) and 0.1 (95% CF). As illustrated in Fig. 8, the new parameter does not correlate with the redshift of reionization z_{rei} but because it increases the total τ_e it correlates with σ_8 and n_s , increasing their values with respect to the ones quoted by the WMAP3 team (Spergel et al. 2006). Invoking a non-standard recombination history may ease the tension between the low value of $\sigma_8 \sim 0.74$ from the WMAP3 analysis (assuming standard recombination history) and clusters data that instead seem to favor larger values of $\sigma_8 \sim 0.9$ (Evrard et al. 2007), but see (Bode et al. 2007).

Using the results of the simulations presented in § 5 that are approximately summarized by equation (42), we are able to constrain the abundance of PBHs with masses $1 M_\odot < M_{pbh} < 10^8 M_\odot$. The results are shown by the thick solid line in Fig. 9(left).

6.2. Spectral Distortions

The injection of some form of energy density, ΔU , in the expanding universe at redshifts $z < 10^7$ cannot be fully thermalized, and so it produces observable deviations of the CMB spectrum from a perfect black-body (*e.g.*, Burigana et al. 1991). There are two types of spectral distortions: μ and y -distortions. Energy injection in the redshift range $10^7 < z < 10^5$ produces a Bose-Einstein spectrum with chemical potential $\Delta U/U = 0.71\mu$, where U is the unperturbed energy density of the CMB. In the redshift interval $10^5 < z < 1000$

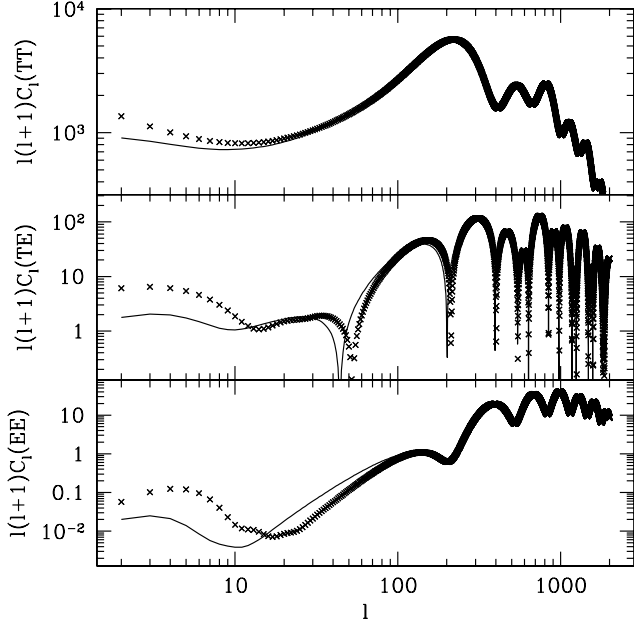


FIG. 7.— Power spectrum of temperature and polarization anisotropies for the best fit WAMP3 model with $\tau_e = 0.09$ and redshift of reionization $z_{rei} = 11$ (crosses) and a model with the same τ_e but $z_{rei} = 7$ and modified recombination history with constant residual ionization fraction $x_{e0} = 2.5 \times 10^{-3}$. The panels show from top to bottom: TT, EE and TE power spectra.

the Comptonization distortion dominates and has amplitude $\Delta U/U = 4y$. Using the spectrometer FIRAS on the COBE satellite, Fixsen et al. (1996) found the following upper limits for the deviation of the CMB from a Planck spectrum: $\mu \leq 9 \times 10^{-5}$ and $y \leq 1.5 \times 10^{-5}$ at 95% confidence. It follows that $\Delta U/U \leq 6 \times 10^{-5}$ at 95% confidence from $10^7 < z < 1000$. In this section we calculate the value of the y -parameter produced by a population of PBHs of mass M_{pbh} and compare it to observed upper limits from FIRAS to set upper limits on their abundance. In order to calculate the total value of the y -parameter we need to distinguish between three epochs for the energy injection:

1) Before the redshift of last scattering at $z_{rec} \sim 1000$ the universe is optically thick to Compton scattering hence all the energy emitted by accreting PBHs is absorbed by the cosmic gas. During this epoch the y -parameter is

$$y_1 = \frac{1}{4U(z_{eq})} \int_{z_{eq}}^{z_{rec}} \frac{dz}{aH(z)} \frac{d\Delta U(z)}{dt} \quad (44)$$

where $d\Delta U(z)/dt$ is the total energy per unit comoving volume per unit time emitted by accretion onto PBHs and $U(z)$ is the unperturbed comoving energy density of the CMB at redshift z . We will show that this contribution to the total y -parameter is dominant. We integrate $d\Delta U(z)/dt$ starting at the redshift of matter-radiation equality because before z_{eq} the effective cosmic sound speed approaches the value $c_s \sim c/\sqrt{3}$ and the gas accretion rate onto PBHs is negligible.

2) Between last scattering and decoupling the estimate of the y -parameter is complicated by the fact that only a fraction of the energy emitted by PBHs is absorbed by the gas and exchanged with the CMB radiation. As a zero-th order approximation we can use equation (44), integrating between z_{dec} and z_{rec} , to estimate an upper

limit for the y -distortion. The integration shows that for PBH masses $M_{pbh} < 10^3 M_\odot$, $y_2 \ll y_1$ even when we assume that all the energy is absorbed by the gas. In § 4.2.1 we estimated that only a fraction $C \sim 1.4 \times 10^{-4}$ of the radiation emitted by PBHs is deposited into heat. A more realistic estimate of ΔU is obtained by multiplying our upper limit for y_2 by C . Hence, we do not need to worry further about getting a more precise estimate of y_2 for PBH of any mass as $y_2 \ll y_1$.

3) After decoupling Compton heating/cooling becomes negligible and we can calculate the y -parameter using the relationship:

$$y_3 = \frac{k_B}{m_e c^2} \int_{z_{dec}}^{10} (T_e - T_{cmb}) d\tau_e. \quad (45)$$

Let's estimate the upper limit for y_3 . Assuming $T_e = \text{constant} \gg T_{cmb}$ we have $y_3 = 1.726 \times 10^{-6} (T_e/10^4 \text{ K}) \Delta\tau_e$. In all the models consistent with WMAP3 data the gas temperature is $T_e < 1000 \text{ K}$ and $\Delta\tau_e$ between redshift $z \sim 10$ and $z \sim 100$ is < 0.05 . It follows that the upper limit on y_3 is 8.6×10^{-9} which is negligible when compared to the FIRAS upper limit. Finally, the value of the y -parameter is the sum of the y during each epoch. Thus, in our case, we have $y \approx y_1$.

Let's now estimate y_1 . The total energy density emitted per unit time per unit comoving volume is $\Delta U/dt = l L_{Ed} n_{pbh}$. Thus we find

$$y_1 = \frac{L_{Ed} \rho_{crit} \Omega_{dm}}{4M_{pbh} a_R T_0^4 (1+z_{eq})} f_{pbh} \int_{z_{eq}}^{z_{rec}} dz \frac{l(M_{pbh}, z)}{aH(z)}. \quad (46)$$

Using equation (30) for the dimensionless accretion luminosity l (see also Fig. 4), we obtain the value of the y -parameter as a function of M_{pbh} and f_{pbh} . Imposing $y \leq 1.5 \times 10^{-5}$ we obtain upper limits for $f_{pbh}(M_{pbh})$ at 95% confidence. The results are summarized in Fig. 9(left).

In summary, before the redshift of recombination gas accretion onto PBHs with mass $< 100 M_\odot$ is not greatly reduced by Compton drag. Although the accretion luminosity during this epoch does not contribute to increase τ_e , the energy injection produce spectral distortions of the CMB, increasing the value of the y -parameter. We find that the existence of PBHs with masses $< 100 M_\odot$ is best constrained by upper limits on the y -parameter from FIRAS.

7. DISCUSSION AND SUMMARY

During the radiation era, mildly non-linear perturbations with $\delta\rho/\rho \sim 0.5 - 1$ can collapse directly into primordial black holes (PBHs). Such black holes may have masses ranging from the Planck mass to a million solar masses, depending on the redshift of their formation and the details of the formation mechanism. The abundance of evaporating PBHs with masses $< 10^{15} \text{ g}$ is constrained by observations to be a fraction $\beta \lesssim 10^{-22}$ of the mean energy density of the universe at the time of their formation, but the existence of PBHs with masses larger than 10^{15} g is poorly constrained. It is not ruled out that the bulk of the dark matter may be composed of PBHs with masses in the range between 10^{15} g and 10^{26} g or Planck mass relics with $M \sim 10^{-5} \text{ g}$. In this work, the last of a series of three papers, we study the effects of a (yet undetected) population of non-evaporating PBHs on the

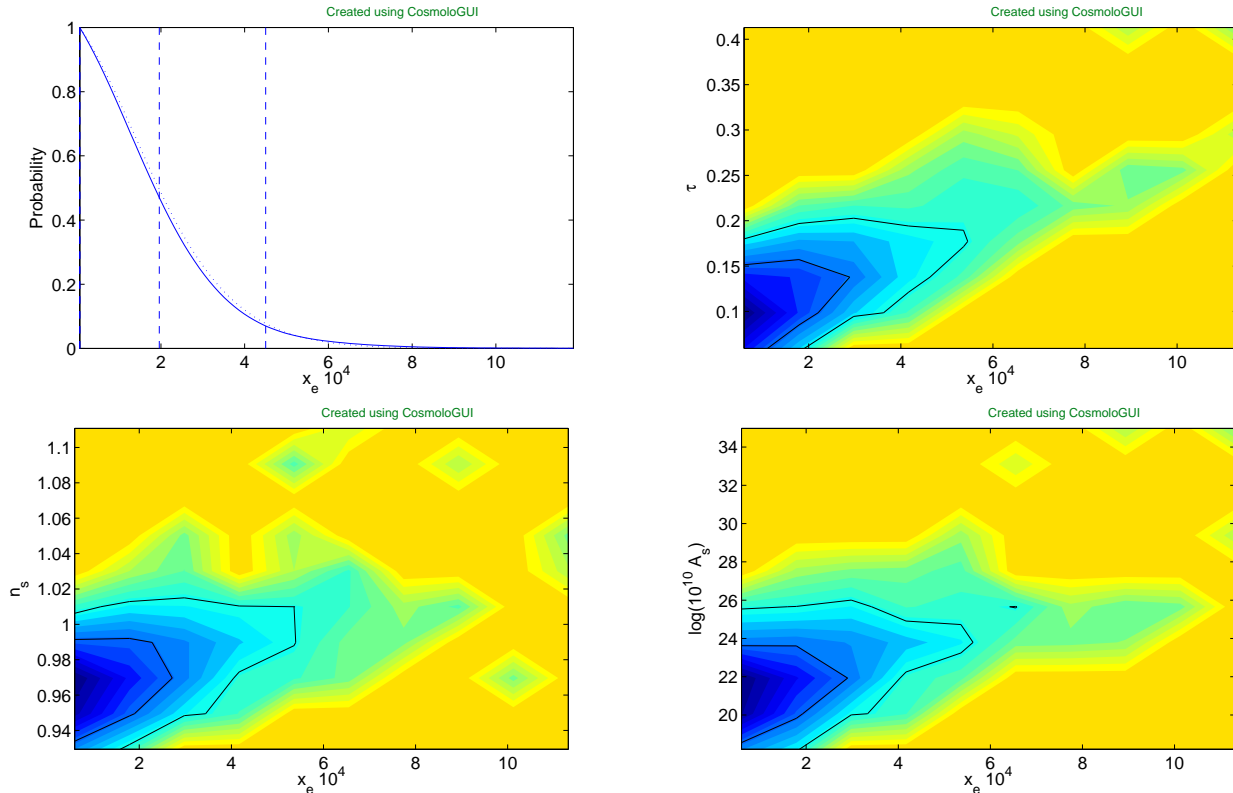


FIG. 8.— Likelihood isocontours of cosmological parameters as a function of x_{e0} which describes the modified recombination history produced by PBHs (see the text). We have used WMAP3 data and a modified version of COSMOMC (Lewis & Bridle 2002). The equation used for the non-standard recombination history is given in equation (43) and the free parameter x_{e0} describes the electron fraction at $z = 1000$. The four panels from the top-left corner show (clockwise): i) marginalized likelihood of x_{e0} (in units of 10^{-4}) with 68% and 95% confidence limits; ii) optical depth τ_e vs x_{e0} ; iii) amplitude of the power spectrum vs x_{e0} ; iv) scalar tilt of the initial power spectrum depth n_s vs x_{e0} .

thermal and ionization history of the universe and their signatures on the CMB anisotropies and spectrum. In Paper I we focused on studying the formation and growth of the dark matter halo which envelopes PBHs that do not constitute the bulk of the dark matter. In the second paper (Ricotti 2007), we study in detail the Bondi-type accretion solutions onto PBHs including the effects of Compton drag, Hubble expansion and the growth of the dark matter halo. Finally, this work focuses on modeling the accretion luminosity of PBHs including feedback effects and observational signatures.

We find that if a fraction f_{pbh} of the dark matter is in PBHs with mass $> 0.1 M_{\odot}$, the energy released due to gas accretion may produce spectral distortions of the CMB radiation and keep the universe partially ionized after recombination. The limits on the mass and abundances of PBHs set from observations of the X-ray background are much less restrictive than those from the CMB. The modified recombination history produces observable signatures on the spectrum of polarization anisotropies of the CMB at angular scales $l \gtrsim 10$. Hence, the effect of PBHs cannot be confused with the effect of ionization by high redshift galaxies which affect polarization anisotropies on larger angular scales.

We are able to improve the constraints on f_{pbh} for PBHs with masses $> 0.1 M_{\odot}$ by several orders of magnitude using WMAP3 and FIRAS data. The results are summarized in Fig. 9 (left). The upper limits on the abundance of PBHs with masses $0.1 M_{\odot} < M_{pbh} < 10^8 M_{\odot}$ at the epoch of their formation, β , are shown in Fig. 9

(right). We use equation (1) to derive β as a function of M_{pbh} , f_{pbh} and the ratio $f_{Hor} = M_{pbh}/M_H$ between the PBH mass and the mass M_H of the horizon at the epoch of PBH formation.

Fitting WMAP3 data with cosmological models that do not allow for non-standard recombination histories as produced by PBHs or other early energy sources may lead to an underestimate of the best-fit values of the amplitude of linear density fluctuations, σ_8 , and the scalar spectral index, n_s . This happens because the contribution of PBHs to the optical depth to Thomson scattering, which is uncorrelated with the contribution from galactic ionization sources, can be $\Delta\tau_e \lesssim 0.05$ ($\Delta\tau_e \lesssim 0.1$ at 95% CF). Since n_s and σ_8 are correlated with τ_e , their best fit values may increase to $n_s \sim 1$ and $\sigma_8 \sim 0.9$ (at 95% CF). This is a general result that may reduce recent tensions between WMAP3 data and clusters data on the value of σ_8 (Evrard et al. 2007).

A population of intermediate mass black holes (IMBHs) with masses of about $100 - 1000 M_{\odot}$ is still allowed and may be widespread if a fraction of the ultraluminous X-ray sources (ULX) observed in nearby galaxies host IMBHs (Miller et al. 2003; Dewangan et al. 2006). The origin of IMBHs is unknown, but if they are produced by Pop III stars their number may fall short in explaining the observed ULXs population (e.g., Kuranov et al. 2007; Pelupessy et al. 2007). We find that, if all or a fraction of observed ULXs are PBHs with masses $M_{pbh} \sim 100 - 1000 M_{\odot}$ with $f_{pbh} \sim 10^{-5}$, they would increase the best fit value of the optical depth to

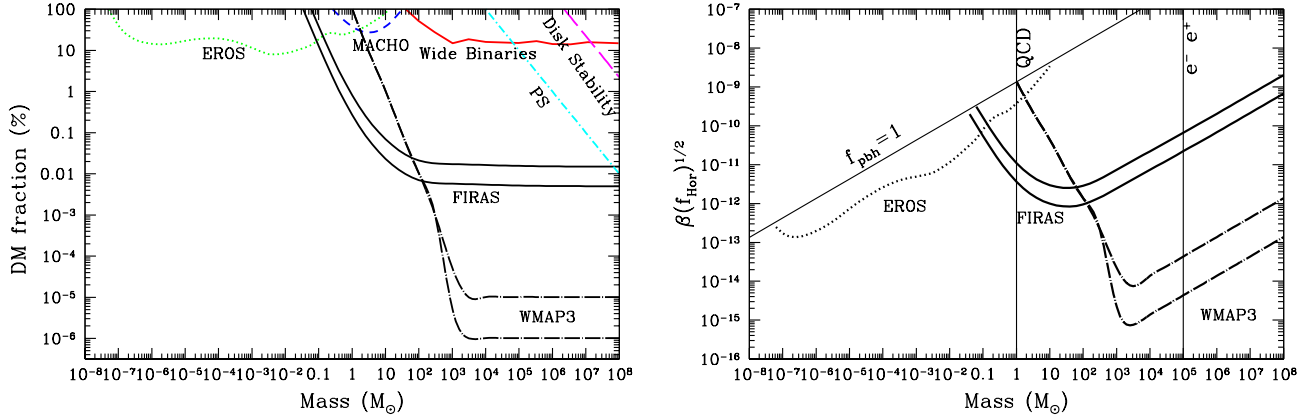


FIG. 9.— (left) Upper limits on the present abundance of PBHs. The thick lines are the results obtained in the present work. The solid lines show the upper limits using WMAP3 data (CMB anisotropies) for two values of the black hole duty cycle $f_{duty} = 1$ and 0.1 . The dashed lines show the limits using FIRAS data (CMB spectral distortions) at 95% and 68% confidence. The other lines refer to previous upper limits from microlensing (EROS and MACHO experiments) and dynamical constraints (see introduction). (Right) Upper limits on the abundance of PBHs at the epoch of their formation β as a function of their mass. We assume that the mass of PBHs is a fraction f_{Hor} of the mass of the horizon at the epoch of their formation. The thick curves show the upper limits obtained in the present work and the thin dotted curve are limits from the EROS collaboration (microlensing experiment).

Thompson scattering to $\tau_e \sim 0.2$. Since the scalar spectral index n_s and the amplitude of density fluctuations A_s and σ_8 are correlated to τ_e , their best fits also increase to $n_s \sim 1$ and $\sigma_8 \sim 0.9$. PBHs in this mass range may be produced in two-stage inflationary models designed to fit the low WMAP quadrupole (Kawasaki et al. 2006). We emphasize again that this effect is more general than the specific case of PBHs discussed in this paper. Any mechanism or energy source that modifies the standard recombination history may affect the estimate of cosmological parameters in a way similar to that discussed here.

Our results are in contradiction with the suggestion that MACHOs are PBHs with mass $\sim 0.1 - 1 M_\odot$ and $f_{pbh} \sim 0.2$ (Alcock et al. 2000). Such a PBH population would produce spectral distortions incompatible with FIRAS data.

The luminous QSOs found by SLOAN at $z \sim 6$ are thought to be powered by $10^8 - 10^9 M_\odot$ SMBHs. It is difficult to produce such massive black holes starting from small seeds by gas accretion because the age of the universe at $z = 6$ is a few tens the Salpeter accretion timescale. A few massive PBHs or numerous less massive PBHs may help explain the origin of SMBHs at high redshift and in present day galaxies by producing relatively massive “seeds”. Are the upper limits on the number of PBHs derived in this work compatible with this scenario? The fraction of mass in SMBHs today is approximately $\Omega_{smbh}/\Omega_{dm} \sim 2.13 \times 10^{-5}$ (Gebhardt et al. 2000; Ricotti & Ostriker 2004). For PBHs with mass $> 1000 M_\odot$ we found $f_{pbh} = \Omega_{pbh}/\Omega_{dm} \lesssim 10^{-6}/f_{duty}$. Hence, assuming that only a fraction $F_{agn} \leq 1$ of PBHs is incorporated into SMBHs and grows by gas accretion by a factor $X_{acc} \geq 1$ we have: $f_{pbh} X_{acc} F_{agn} \sim 2 \times 10^{-5}$ or $X_{acc} F_{agn} \gtrsim 20 f_{duty}$. The most massive PBHs have $F_{agn} \rightarrow 1$ because they spiral in to the centers of galaxies by dynamical friction on a shorter timescale ($t_{fric}/t_H(z) \sim 0.02 M_{halo}(z)/M_{pbh}$, where t_H is the Hubble time) and because they may accrete gas more efficiently. Hence, for $f_{duty} \sim 3\%$ and $F_{agn} = 1$ we find $X_{acc} \gtrsim 1$ indicating that even scenarios with negligible mass accretion onto PBHs (*i.e.*, only growth through mergers) are consistent with the observed mass

in SMBHs today.

Less massive PBHs have lower probability for growing to masses typical of SMBHs because the Bondi accretion rate is $\propto M^2$. However, the upper limit on the abundance of PBHs increases steeply with decreasing mass for $M_{pbh} < 1000 M_\odot$. Thus, although a smaller fraction of the seed PBHs can grow substantially, the number of seeds available can be much larger. PBHs with masses smaller than $100 M_\odot$, assuming Bondi type accretion from the ISM of a typical high- z galaxy, are unlikely to accrete rapidly enough to grow to SMBH masses in less than 1 Gyr, even if they constitute a few per cent of the dark matter (Kuranov et al. 2007; Pelupessy et al. 2007; Ricotti & Köckert 2007).

The increased fractional ionization of the cosmic gas produced by non-standard recombination also increases the primordial molecular hydrogen abundance to $x_{H_2} \sim 10^{-4} - 10^{-5}$ after redshift $z \sim 100$. This value is between ten and one hundred times larger than the standard value, $x_{H_2} \sim 10^{-6}$, obtained neglecting PBHs. The increase of the cosmic Jeans mass due to X-ray heating is negligible for models consistent with the CMB data. Therefore, the formation rate of the first galaxies and stars may be enhanced if a population of PBHs exists. Several aspects of first-star and galaxy-formation physics would be affected by the enhanced molecular fraction: (i) the mass of the first stars may be reduced due to formation of HD molecules (Nagakura & Omukai 2005); (ii) the intergalactic medium would be optically thick to H_2 photo-dissociating radiation in the Lyman-Werner bands, allowing molecular hydrogen to survive in the low density IGM even at relatively low redshifts $z \sim 10 - 15$; (iii) the epoch of domination of the first stars and galaxies would probably start earlier and perhaps last longer. The number of first galaxies that remain completely dark would be reduced. It is not obvious that the star formation efficiency and other internal properties of the first galaxies would be affected because feedback effects such as photo-evaporation from internal sources and SN explosions are probably dominant (Ricotti et al. 2002a,b). We leave quantitative calculations on the impact of PBHs on the formation of the first galaxies to a future work.

ACKNOWLEDGMENTS

MR acknowledge stimulating discussions with Niayesh Afshordi, Carlo Burigana, Andrea Ferrara, Avi Loeb, Cole Miller, Eve Ostriker, Ruben Salvaterra, David

Spergel and Mathias Zaldariaga. This work was supported in part by NASA grant NNX07AH10G (MR) and a NSF Graduate Research Fellowship (KJM).

REFERENCES

- Afshordi, N., McDonald, P., & Spergel, D. N. 2003, *ApJ*, 594, L71
 Alcock, C., et al. 1998, *ApJ*, 499, L9
 Alcock, C., et al. 2000, *ApJ*, 542, 281
 Alcock, C., et al. 2001, *ApJ*, 550, L169
 Alexander, S., & Mészáros, P. 2007, *ArXiv High Energy Physics - Theory e-prints*
 Battistelli, E. S., Fulcoli, V., & Macculi, C. 2000, *New Astronomy*, 5, 77
 Bertschinger, E. 1985, *ApJS*, 58, 39
 Bicknell, G. V., & Henriksen, R. N. 1978, *ApJ*, 225, 237
 Bode, P., Ostriker, J. P., Weller, J., & Shaw, L. 2007, *ApJ*, 663, 139
 Bondi, H., & Hoyle, F. 1944, *MNRAS*, 104, 273
 Burigana, C., Danese, L., & de Zotti, G. 1991, *A&A*, 246, 49
 Carr, B. 1994, *ARA&A*, 32, 531
 Carr, B. J. 1975, *ApJ*, 201, 1
 Carr, B. J. 1981, *MNRAS*, 194, 639
 Carr, B. J. 2003, *LNP Vol. 631: Quantum Gravity: From Theory to Experimental Search*, 631, 301
 Carr, B. J. 2005, *ArXiv Astrophysics e-prints*
 Carr, B. J., & Hawking, S. W. 1974a, *MNRAS*, 168, 399
 Carr, B. J., & Hawking, S. W. 1974b, *MNRAS*, 168, 399
 Chisholm, J. R. 2006, *Phys. Rev. D*, 73, 083504
 Chiu, W. A., & Ostriker, J. P. 2000, *ApJ*, 534, 507
 Chongchitnan, S., & Efstathiou, G. 2007, *Journal of Cosmology and Astro-Particle Physics*, 1, 11
 Choptuik, M. W. 1993, *Physical Review Letters*, 70, 9
 Dewangan, G. C., Titarchuk, L., & Griffiths, R. E. 2006, *ApJ*, 637, L21
 Dokuchaev, V., Eroshenko, Y., & Rubin, S. 2004, *ArXiv Astrophysics e-prints*
 Evans, C. R., & Coleman, J. S. 1994, *Physical Review Letters*, 72, 1782
 Evrard, A. E., et al. 2007, *ArXiv Astrophysics e-prints*
 Fixsen, D. J., Cheng, E. S., Gales, J. M., Mather, J. C., Shafer, R. A., & Wright, E. L. 1996, *ApJ*, 473, 576
 Gebhardt, K., et al. 2000, *ApJ*, 539, L13
 Gnedin, N. Y., Ostriker, J. P., & Rees, M. J. 1995, *ApJ*, 438, 40
 Green, A. M., Liddle, A. R., Malik, K. A., & Sasaki, M. 2004, *Phys. Rev. D*, 70, 041502
 Guedens, R., Clancy, D., & Liddle, A. R. 2002a, *Phys. Rev. D*, 66, 083509
 Guedens, R., Clancy, D., & Liddle, A. R. 2002b, *Phys. Rev. D*, 66, 43513
 Hamadache, C., et al. 2006, *A&A*, 454, 185
 Harada, T., & Carr, B. J. 2005, *Phys. Rev. D*, 71, 104009
 Hawking, S. 1971, *MNRAS*, 152, 75
 Hawking, S. W. 1974, *Nature*, 248, 30
 Jedamzik, K. 1997, *Phys. Rev. D*, 55, 5871
 Jin, S., Ostriker, J. P., & Wilkinson, M. I. 2005, *MNRAS*, 359, 104
 Kawasaki, M., Takayama, T., Yamaguchi, M., & Yokoyama, J. 2006, *Phys. Rev. D*, 74, 043525
 Khlopov, M. Y., Rubin, S. G., & Sakharov, A. S. 2005, *Astroparticle Physics*, 23, 265
 Kuranov, A. G., Popov, S. B., Postnov, K. A., Volonteri, M., & Perna, R. 2007, *MNRAS*, 377, 835
 Lacey, C. G., & Ostriker, J. P. 1985, *ApJ*, 299, 633
 Lewis, A., & Bridle, S. 2002, *Phys. Rev. D*, 66, 103511
 Lin, D. N. C., Carr, B. J., & Fall, S. M. 1976, *MNRAS*, 177, 51
 Loeb, A. 1993, *ApJ*, 403, 542
 Mack, K., Ostriker, J., & Ricotti, M. 2007, *ApJ*, in press, astro-ph/Majumdar, A. S. 2003, *Physical Review Letters*, 90, 031303
 Meszaros, P. 1975a, *A&A*, 38, 5
 Meszaros, P. 1975b, *A&A*, 44, 59
 Miller, J. M., Fabbiano, G., Miller, M. C., & Fabian, A. C. 2003, *ApJ*, 585, L37
 Miller, M. C., & Ostriker, E. C. 2001, *ApJ*, 561, 496
 Moore, B. 1993, *ApJ*, 413, L93
 Musco, I., Miller, J. C., & Rezzolla, L. 2005, *Classical and Quantum Gravity*, 22, 1405
 Nagakura, T., & Omukai, K. 2005, *MNRAS*, 364, 1378
 Narayan, R., & Yi, I. 1995, *ApJ*, 452, 710
 Nozari, K. 2007, *Astroparticle Physics*, 27, 169
 Ostriker, J. P., & Suto, Y. 1990, *ApJ*, 348, 378
 Park, M.-G., & Ostriker, J. P. 2001, *ApJ*, 549, 100
 Peluassy, F. I., Di Matteo, T., & Ciardi, B. 2007, *ArXiv Astrophysics e-prints*
 Polnarev, A., & Zembowicz, R. 1991, *Phys. Rev. D*, 43, 1106
 Press, W. H., & Schechter, P. 1974, *ApJ*, 193, 437
 Ricotti, M. 2007, *ApJ*, 662, 53
 Ricotti, M., Gnedin, N. Y., & Shull, J. M. 2001, *ApJ*, 560, 580
 Ricotti, M., Gnedin, N. Y., & Shull, J. M. 2002a, *ApJ*, 575, 33
 Ricotti, M., Gnedin, N. Y., & Shull, J. M. 2002b, *ApJ*, 575, 49
 Ricotti, M., & Köckert, F. 2007, in preparation
 Ricotti, M., & Ostriker, J. P. 2004, *MNRAS*, 352, 547
 Rubin, S. G., Sakharov, A. S., & Khlopov, M. Y. 2001, *Soviet Journal of Experimental and Theoretical Physics*, 92, 921
 Seager, S., Sasselov, D. D., & Scott, D. 1999, *ApJ*, 523, L1
 Shapiro, S. L. 1973a, *ApJ*, 180, 531
 Shapiro, S. L. 1973b, *ApJ*, 185, 69
 Shapiro, S. L., Lightman, A. P., & Eardley, D. M. 1976, *ApJ*, 204, 187
 Shapley, A. E., Steidel, C. C., Pettini, M., & Adelberger, K. L. 2003, *ApJ*, 588, 65
 Silk, J. 1968, *ApJ*, 151, 459
 Spergel, D. N., et al. 2006, *ArXiv Astrophysics e-prints*
 Stojkovic, D., Freese, K., & Starkman, G. D. 2005, *Phys. Rev. D*, 72, 045012
 Tikhomirov, V. V., & Tsalkou, Y. A. 2005, *Phys. Rev. D*, 72, 121301
 Umemura, M., Loeb, A., & Turner, E. L. 1993, *ApJ*, 419, 459
 Yoo, J., Chanamé, J., & Gould, A. 2004, *ApJ*, 601, 311
 Zel'Dovich, Y. B., & Novikov, I. D. 1967, *Soviet Astronomy*, 10, 602